



HAL
open science

Broadband seismic monitoring of active volcanoes using deterministic and stochastic approaches

Hiroyuki Kumagai, Masaru Nakano, Takuto Maeda, Hugo Yepes, Pablo Palacios, Mario Ruiz, Santiago Arrais, Mayra Vaca, Indira Molina, Tadashi Yamashima

► **To cite this version:**

Hiroyuki Kumagai, Masaru Nakano, Takuto Maeda, Hugo Yepes, Pablo Palacios, et al.. Broadband seismic monitoring of active volcanoes using deterministic and stochastic approaches. *Journal of Geophysical Research : Solid Earth*, 2010, 115, pp.1815-1827. 10.1029/2009JB006889 . insu-03596890

HAL Id: insu-03596890

<https://insu.hal.science/insu-03596890>

Submitted on 4 Mar 2022

HAL is a multi-disciplinary open access archive for the deposit and dissemination of scientific research documents, whether they are published or not. The documents may come from teaching and research institutions in France or abroad, or from public or private research centers.

L'archive ouverte pluridisciplinaire **HAL**, est destinée au dépôt et à la diffusion de documents scientifiques de niveau recherche, publiés ou non, émanant des établissements d'enseignement et de recherche français ou étrangers, des laboratoires publics ou privés.

Copyright

Broadband seismic monitoring of active volcanoes using deterministic and stochastic approaches

Hiroyuki Kumagai,¹ Masaru Nakano,¹ Takuto Maeda,^{1,3} Hugo Yepes,² Pablo Palacios,² Mario Ruiz,² Santiago Arrais,² Mayra Vaca,² Indira Molina,^{2,4} and Tadashi Yamashima¹

Received 19 August 2009; revised 21 December 2009; accepted 22 February 2010; published 3 August 2010.

[1] We systematically used two approaches to analyze broadband seismic signals for monitoring active volcanoes: one is waveform inversion of very-long-period (VLP) signals assuming possible source mechanisms; the other is a source location method of long-period (LP) events and tremor using their amplitudes. The deterministic approach of the waveform inversion is useful to constrain the source mechanism and location but is basically only applicable to VLP signals with periods longer than a few seconds. The source location method assumes isotropic radiation of *S* waves and uses seismic amplitudes corrected for site amplifications. This simple approach provides reasonable source locations for various seismic signals such as a VLP event accompanying LP signals, an explosion event, and tremor associated with lahars and pyroclastic flows observed at five or fewer stations. Our results indicate that a frequency band of about 5–12 Hz and a *Q* factor of about 60 are appropriate for the determination of the source locations. In this frequency band the assumption of isotropic radiation may become valid because of the path effect caused by the scattering of seismic waves. The source location method may be categorized as a stochastic approach based on the nature of scattering waves. Systematic use of these two approaches provides a way to better utilize broadband seismic signals observed at a limited number of stations for improved monitoring of active volcanoes.

Citation: Kumagai, H., M. Nakano, T. Maeda, H. Yepes, P. Palacios, M. Ruiz, S. Arrais, M. Vaca, I. Molina, and T. Yamashima (2010), Broadband seismic monitoring of active volcanoes using deterministic and stochastic approaches, *J. Geophys. Res.*, *115*, B08303, doi:10.1029/2009JB006889.

1. Introduction

[2] Broadband seismic instruments introduced to observe active volcanoes in the early 1990s have led to innovative approaches in the study of active volcanism. Broadband observations have revealed that very-long-period (VLP) signals, with periods longer than a few seconds, are widely observed in relation to magmatic and hydrothermal activity [e.g., Kawakatsu *et al.*, 1992, 1994, 2000; Neuberg *et al.*, 1994; Kaneshima *et al.*, 1996; Chouet *et al.*, 1999]. The finding of VLP signals has stimulated the development of waveform inversion methods suitable for the analysis of these signals [e.g., Ohminato *et al.*, 1998; Nakano and Kumagai, 2005; Auger *et al.*, 2006]. Quantitative analyses of VLP

signals based on waveform inversions have been successfully used to investigate dynamic magmatic and hydrothermal processes [e.g., Ohminato *et al.*, 1998; Legrand *et al.*, 2000; Nishimura *et al.*, 2000; Kumagai *et al.*, 2001, 2003; Chouet *et al.*, 2003, 2005; Ohminato, 2006; Waite *et al.*, 2008; Kobayashi *et al.*, 2009]. Broadband seismic observations also have been used for real-time monitoring of active volcanoes [e.g., Dawson *et al.*, 2004; Auger *et al.*, 2006; Kumagai *et al.*, 2007]. Auger *et al.* [2006] applied waveform inversion to make real-time estimations of source locations and mechanisms of VLP signals at Stromboli volcano, Italy, using a network of 13 broadband seismic stations at this volcano.

[3] Although waveform inversion is useful to study and monitor active volcanoes, its application is basically limited to VLP signals with periods longer than a few seconds. It is difficult to apply a waveform inversion to long-period (LP) events and tremor with periods shorter than 1 s. This difficulty originates in our poor knowledge of small-scale structural heterogeneities for correct estimations of Green's functions. Lockmer *et al.* [2007] and Bean *et al.* [2008] indicated that near-surface volcano structure seriously affects waveform inversion results of LP signals. Although Kumagai *et al.* [2002] and Nakano *et al.* [2003] performed

¹Earthquake Research Department, National Research Institute for Earth Science and Disaster Prevention, Tsukuba, Japan.

²Instituto Geofísico, Escuela Politécnica Nacional, Quito, Ecuador.

³Now at Center for Integrated Disaster Information Research, Interfaculty Initiative in Information Studies, The University of Tokyo, Tokyo, Japan.

⁴Now at Institut des Sciences de la Terre d'Orléans, Orleans, France.

waveform inversions of LP events with periods of about 1 s at Kusatsu-Shirane volcano, Japan, the inversions were relatively easy because the seismic network at this volcano was within 1 km of the epicenters of the LP events. Similarly, the waveform inversion of an LP event at Kilauea, Hawaii, was observed by a dense network located at epicentral distances of 1–2 km [Kumagai *et al.*, 2005]. The influence of small-scale structural heterogeneities on a waveform inversion of LP signals may become significant when epicentral distances are greater than a few kilometers as shown by the synthetic tests by *Bean et al.* [2008]. Such networks are commonly used to monitor active volcanoes. It would be very difficult to accurately estimate the sub-kilometer structural heterogeneities that affect LP signals with periods shorter than 1 s. Therefore, it seems hopeless to apply a waveform inversion approach to LP and tremor signals observed by ordinary seismic networks on active volcanoes, although these signals are frequently observed in association with heightened volcanic activity. We may need another approach to better utilize broadband seismic signals for estimating source parameters of LP events and tremor in periods shorter than 1 s.

[4] Because LP events and tremor have emergent onsets, traditional hypocenter determinations using onset arrival times are usually difficult or impossible. As an alternative to the use of arrival times, *Battaglia and Aki* [2003] proposed an approach to locate LP events and tremor using their amplitudes based on the method originally proposed by *Yamasato* [1997]. This simple approach was successful in locating rockfalls, LP events, and fissure eruptions, offering the potential for routine and automatic determinations of source locations of LP events and tremor. *Battaglia and Aki* [2003] assumed isotropic wave radiation for LP events and tremor. However, LP events and tremor are interpreted as the resonances of fluid-filled resonators [e.g., *Chouet*, 1996a], and the waveform inversion studies on LP events cited above indicate that a crack geometry is the most appropriate for the LP source. The assumption of isotropic wave radiation used by *Battaglia and Aki* [2003] is apparently inconsistent with the hypothesis of a crack geometry at the LP source. This inconsistency should be addressed before the use of their approach.

[5] In this paper we first discuss the justification and limitations of the method of *Battaglia and Aki* [2003]. We show that this method relies on the path effect of scattered waves and may be valid only in a high-frequency range. This method thus may be categorized as a stochastic approach that is based on the nature of scattered waves. We apply this stochastic approach, as well as the deterministic approach based on waveform inversion, to broadband seismic signals observed at Cotopaxi and Tungurahua volcanoes, Ecuador. On each volcano, five observation stations feature broadband seismometers and infrasonic sensors located 1–5 km from the summit. We demonstrate that broadband seismic data from such a limited number of stations are useful to quantify source parameters of VLP and LP events and tremor using the two approaches. We present analysis results of a VLP event accompanying LP signals, an explosion event, tremor signals associated with lahars and pyroclastic flows, and VLP signals associated with

eruptions. These approaches provide a way to better utilize broadband seismic signals and are useful to monitor a wide variety of phenomena at active volcanoes.

2. Methods

2.1. Source Representation

[6] The displacement field excited by a point source assuming a moment tensor may be written as

$$u_i(t) = \sum_{j=1}^6 m_j(t) * G_{ij}(t), \quad (1)$$

where G_{ij} is the spatial derivative of Green's function, m_j is the moment tensor function, and the asterisk denotes convolution [e.g., *Aki and Richards*, 1980]. The moment tensor function m_j can be decomposed into the moment tensor M and moment function s as follows:

$$M(t) = s(t) \begin{bmatrix} M_{11} & M_{12} & M_{13} \\ M_{12} & M_{22} & M_{23} \\ M_{13} & M_{23} & M_{33} \end{bmatrix} \quad (2)$$

and

$$\begin{aligned} & [m_1(t), m_2(t), m_3(t), m_4(t), m_5(t), m_6(t)] \\ & = s(t) [M_{11}, M_{22}, M_{33}, M_{12}, M_{23}, M_{13}]. \end{aligned} \quad (3)$$

The moment tensor M and moment function s for an isotropic source are given by

$$M(t) = s(t) \begin{bmatrix} 1 & 0 & 0 \\ 0 & 1 & 0 \\ 0 & 0 & 1 \end{bmatrix} \quad (4)$$

and

$$s(t) = (\lambda + 2\mu)\Delta V(t), \quad (5)$$

where λ and μ are Lamé's constants and ΔV is the volume change caused by a spherical source [e.g., *Kawakatsu and Yamamoto*, 2007]. The moment tensor M and moment function s for a crack mechanism are given as

$$\begin{aligned} & M(t) = s(t) \\ & \cdot \begin{bmatrix} \lambda/\mu + 2 \sin^2 \theta \cos^2 \theta & 2 \sin^2 \theta \sin \phi \cos \phi & 2 \sin \theta \cos \theta \cos \phi \\ 2 \sin^2 \theta \sin \phi \cos \phi & \lambda/\mu + 2 \sin^2 \theta \sin^2 \phi & 2 \sin \theta \cos \theta \sin \phi \\ 2 \sin \theta \cos \theta \cos \phi & 2 \sin \theta \cos \theta \sin \phi & \lambda/\mu + \cos^2 \theta \end{bmatrix} \end{aligned} \quad (6)$$

and

$$s(t) = \mu\Delta V(t), \quad (7)$$

where θ and ϕ are angles defining the normal direction of a crack and ΔV is the volume change of a crack. Here θ is measured from vertical upward to horizontal and ϕ is measured counterclockwise from east [*Chouet*, 1996b].

[7] Using the far-field approximation for a body wave, u_i can be written as

$$u_i(t) = A_0 \dot{s}(t - r_i/\beta) \frac{e^{-Br_i}}{r_i}, \quad (8)$$

where r_i is the distance between the station and the source, and A_0 is the coefficient for the radiation pattern of a body wave, depending on the direction from the source to a station [e.g., *Aki and Richards*, 1980]. Here B is given by

$$B = \frac{\pi f}{Q\beta}, \quad (9)$$

where f is frequency, β is a body-wave velocity, and Q is the quality factor for medium attenuation.

2.2. Locating Long-Period (LP) Events and Tremor Using Amplitudes

[8] *Battaglia and Aki* [2003] used equations (8) and (9) with a constant value of A_0 , without the directional dependence, for the source location determination using seismic amplitudes. These equations with a constant value of A_0 represent an isotropic wave radiation, which is apparently inconsistent with the hypothesis of a crack geometry at the sources of LP events and tremor.

[9] *Liu and Helmberger* [1985] first reported the frequency dependence of S -wave radiation patterns using waveform data of an aftershock event of the 1979 Imperial Valley earthquake. They found that the radiation pattern at low frequencies (<1 Hz) exhibited a four-lobe pattern as expected for a double-couple mechanism, whereas the radiation pattern at higher frequencies (>2 Hz) showed significant distortion from the four-lobe pattern. Recently, *Takemura et al.* [2009] conducted a detailed study of the frequency dependence of S -wave radiation patterns using a large number of waveform data on the main shock and 29 aftershocks of the Tottri-Ken Seibu earthquake ($M_w = 6.6$), Japan. The radiation pattern in a low-frequency range (<2 Hz) was a clear four-lobe pattern, but the pattern in a high-frequency range (>5 Hz) was almost isotropic. *Takemura et al.* [2009] concluded that the path effect caused by the scattering of seismic waves due to small-scale heterogeneities is a major cause of the distortion of the S -wave radiation pattern. As volcanoes have strong structural heterogeneities, such an effect would be significant. If the isotropic radiation assumption of *Battaglia and Aki* [2003] is justified by the path effect caused by the scattering of seismic waves, then their method may be valid only in a high-frequency range.

[10] We apply the method proposed by *Battaglia and Aki* [2003] and *Kumagai et al.* [2009] to determine source locations of LP events and tremor by using their amplitudes (Appendix A). Since high-frequency amplitudes are strongly affected by local site conditions, we correct observed amplitudes by using the coda normalization method [e.g., *Aki and Chouet*, 1975; *Phillips and Aki*, 1986; *Mayedada et al.*, 1991]. It is known that the amplitude ratio of coda waves for lapse times greater than twice the S -wave arrival time recorded at two stations for the same event is free of source and path effects and depends only on the local site amplifications at the two stations. Therefore, site amplification

factors for various stations of a seismic network can be estimated by the ratios of coda amplitudes relative to that of a reference station. We used five frequency ranges (1–6, 3–8, 5–10, 7–12, and 9–14 Hz) for our source location determinations and therefore estimated the coda amplification factors in these five frequency ranges. Although *Battaglia and Aki* [2003], *Battaglia et al.* [2003], and *Kumagai et al.* [2009] used a fixed Q value for their source location determinations, we performed a grid search with respect to the Q value. Therefore, we performed grid searches with respect to the frequency range Q and space for each origin time t_s . We used two schemes for the spatial grid search: in the first we positioned point sources at individual grid nodes spaced 200 m apart on the surface of a volcano (20 × 20 km covering the volcano edifice) by using topographic grid data with a 20 m resolution; in the second we positioned point sources at individual grid nodes spaced 400 m apart in a three-dimensional domain (lateral dimensions of 10 × 10 km and a vertical extent of 4 km) covering a summit.

2.3. Waveform Inversion in the Frequency Domain

[11] We used waveform inversion to quantify the sources of VLP signals. As the number of stations on each volcano is limited to five, we used the waveform inversion method proposed by *Nakano and Kumagai* [2005]. In this method, possible source mechanisms are assumed to reduce the number of free parameters in the waveform inversion, and Akaike's Information Criterion (AIC) [*Akaike*, 1974] is used to select the best model among the possible mechanisms. This procedure permits us to quantify the source mechanism and location with limited waveform data.

[12] Following *Auger et al.* [2006] and *Nakano et al.* [2007, 2008], we performed the waveform inversion in the frequency domain assuming a point source (Appendix B). An estimation of the moment function in a waveform inversion in the time domain [e.g., *Ohminato et al.*, 1998; *Nakano et al.*, 2003] requires a long computation time. This difficulty arises from the convolution relation of the moment function and Green's functions in the time domain, which requires evaluating the entire effect of the time history of the moment function and Green's functions at individual times. The convolution relation in the time domain becomes the multiplication relation in the frequency domain, allowing the solution of the inverse problem to be done separately for each frequency component. Because the dimension of the data kernel matrix in this case is significantly smaller than that in the time domain, we can rapidly solve the inverse problem in the frequency domain, as we show here. Furthermore, the moment function can be simultaneously estimated by the inverse Fourier transform of the frequency components determined by the inversion. Thus, we do not need to assume an elementary source time function used in the inversion in the time domain to reconstruct the moment function [*Ohminato et al.*, 1998; *Nakano et al.*, 2003].

[13] Following *Nakano and Kumagai* [2005], we assumed isotropic and crack mechanisms as possible source mechanisms for our waveform inversion in the frequency domain. Although *Nakano and Kumagai* [2005] assumed a cylindrical (pipe) mechanism, this geometry has never been estimated in previous waveform inversion studies of VLP and LP signals; therefore, we did not assume a pipe geometry in our waveform inversion. We then conducted a

grid search in space to find the best-fit location for an isotropic mechanism and conducted a grid search with respect to θ and ϕ in equation (6) to find the best-fit angles for a crack at a fixed location. We also conducted a grid search in space to find the combination of the best-fit angles and location for a crack. AIC is defined as

$$\text{AIC} = N_c N_f \ln R + 2N_f, \quad (10)$$

where N_f is the number of free parameters. $N_f = N_i$ for an isotropic source and $N_f = N_i + 2$ for a crack. We compared AIC values among possible source mechanisms to select the best model. A difference in AIC > 2 is statistically significant [e.g., Sakamoto *et al.*, 1986].

[14] We estimated Green's functions by using the finite-difference method of *Ohminato and Chouet* [1997] to accommodate the topography of each volcano. We used the reciprocity theorem [e.g., *Aki and Richards*, 1980] to calculate Green's functions efficiently [e.g., *Chouet et al.*, 2005]. We used two computational domains for each volcano in the calculations of Green's functions: one had lateral dimensions of 20×20 km and a vertical extent of 20 km, with a grid of $80 \times 80 \times 80$ m (domain 1), and the other had lateral dimensions of 200×200 km and a vertical extent of 36 km, with a uniform grid of $300 \times 300 \times 300$ m (domain 2). We used domain 1 for the inversions of VLP signals with periods from a few to about 10 s and domain 2 for periods between 10 and 50 s. For calculations of Green's functions with shorter periods, we needed a finer grid to satisfy the criterion of the number of grids per wavelength established by *Ohminato and Chouet* [1997]. For longer periods we needed a larger computational domain to avoid contamination by reflected waves generated at the domain boundaries. Although an absorbing boundary condition [*Clayton and Engquist*, 1977] is used in the finite-difference method of *Ohminato and Chouet* [1997], it is not perfect for absorbing waves, especially those with longer periods. Given limitations in computer memory, we could not use a large computational domain with a finer grid; therefore, we used the two computational domains.

[15] Point sources were positioned at individual grid nodes spaced 240 m apart for domain 1 and 300 m apart for domain 2. In the spatial grid search for the waveform inversion we used an adaptive grid spacing similar to the one proposed by *Dreger et al.* [1998]. In this approach we first used a sparse grid spacing. When the location of a minimum residual lay within a search area, a new search was performed around the location using a reduced grid spacing to find a detailed source location.

3. Data

[16] Networks of stations are maintained at both Cotopaxi and Tungurahua volcanoes (Figures 1a and 1b). Cotopaxi (elevation, 5876 m) is one of the highest glacier-clad active volcanoes in the world. *Barberi et al.* [1995] estimated the average recurrence interval of eruptive episodes of this volcano as 117 years from historical and stratigraphic records over the last 2000 years. Pyroclastic flows during the last major eruption in 1877 melted the summit glaciers, generating lahars that traveled more than 300 km to the Pacific Ocean and devastated surrounding areas. Tungurahua (elevation,

5023 m) has been active since 1999, with activity characterized by vulcanian and strombolian eruptions. In July and August 2006, activity at Tungurahua reached a peak, with vulcanian eruptions accompanied by pyroclastic flows. Since the installation of the broadband seismic and infrasonic network on Tungurahua in July 2006, the number of stations and their locations have changed owing to the effects of eruptions.

[17] Each station includes a broadband seismometer (Guralp CMG-40T: 0.02–60 s) and a low-frequency infrasonic sensor (ACO 7144/4144: 0.01–10 s). The seismometer is placed on a concrete base and buried in sand at a depth of 1–2 m below the ground surface. The infrasonic sensor is covered with foam pads and a plastic cover and attached to a tower 1.5 m above the ground. Seismic and infrasonic waveform data are digitized by a 24 bit data logger (Geotech Smart24D) with a sampling frequency of 50 Hz at each station, then transmitted by a digital telemetry system using 2.4 and 5 GHz wireless LAN to the central office of Instituto Geofísico, Escuela Politécnica Nacional (IG-EPN) in Quito via repeaters (Figure 1c). Two computer servers in the central office receive CD1.1 format packets from the stations at Cotopaxi and Tungurahua and create seismic analysis code (SAC) files 1 min long [*Goldstein et al.*, 2003]. The SAC files are shared by four other Linux computers for data analysis. These waveform data are also transmitted to the National Research Institute for Earth Science and Disaster Prevention in Tsukuba, Japan, via the Internet in nearly real time.

[18] Waveform data from the Cotopaxi and Tungurahua networks are continuously displayed on two Linux computers in IG-EPN using Generic Mapping Tools [*Wessel and Smith*, 1998]. The displays are created in 1 day long raw seismic and infrasonic waveforms, 1 day long band-passed (10–60 s) seismic waveforms, and 1 h long raw seismic waveforms. These displays are shared by the intranet of IG-EPN using a Web browser. We use the automatic event-picking algorithm of *Allen* [1978] and a trigger system using amplitudes of filtered waveforms. In the trigger system we estimate maximum amplitudes of filtered waveforms using the latest 1 min files. If the maximum amplitude at each station during the latest 1 min exceeds a trigger level and if the number of triggered stations in each network exceeds a trigger number, we save the latest 3 min of data as a triggered event. We use two bands for the trigger system, 0.5–3 s (the LP band) and 10–50 s (the VLP band), to trigger LP and VLP events, respectively. The same trigger process is run using the sum of root-mean-square amplitudes of waveforms high-passed at 1 Hz to trigger tremor signals. Trigger levels are set based on noise levels at individual stations.

4. Results

4.1. Site Amplification Factors

[19] We first estimated the coda amplification factors at individual stations of the Tungurahua and Cotopaxi networks. We used BVC2 and BRUN (Figure 1) as the reference stations for the Cotopaxi and Tungurahua networks, respectively. For each volcano, we selected a geographically diverse set of well-recorded regional tectonic earthquakes between January 2008 and March 2009 (Figure 2). At each station we averaged 10 ratios of coda amplitudes measured from these earthquakes to estimate the site amplification

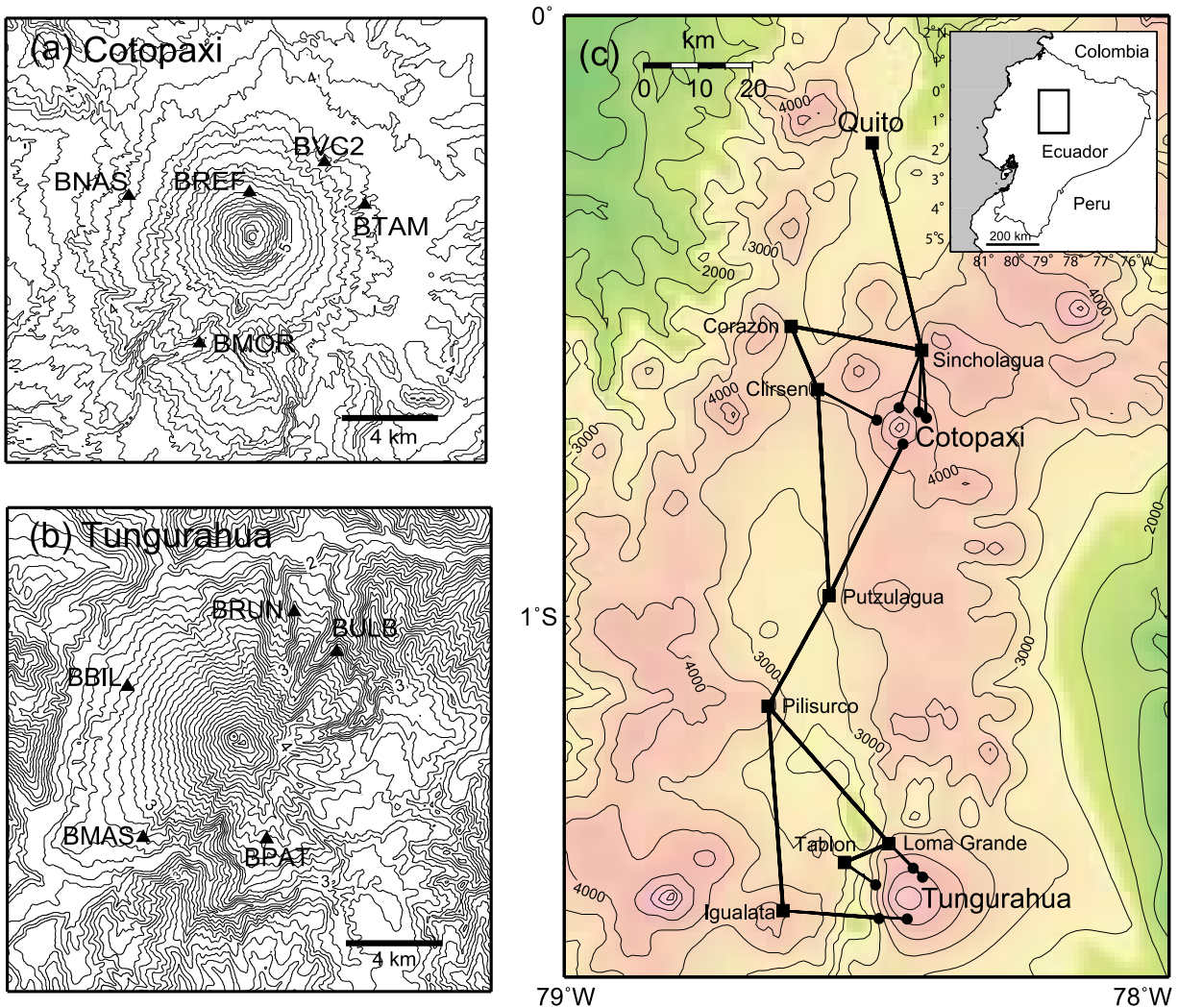


Figure 1. Locations of broadband seismic and infrasonic stations at (a) Cotopaxi and (b) Tungurahua volcanoes. (c) Digital radiotelemetry routes from observation stations at Cotopaxi and Tungurahua (circles) to the central office in Quito via repeaters (squares). Inset map shows the area featured in Figure 1c.

factor. The total number of 10 at each station is smaller than that used in previous studies [e.g., Battaglia and Aki, 2003, Battaglia et al., 2003]. Although we could have used more tectonic earthquakes, additional events tended to occur in similar locations and may have caused deviations in our estimates of site amplification factors. Furthermore, the Tungurahua network was affected by eruptions, and it was difficult to obtain seismograms of a tectonic earthquake recorded simultaneously at all the stations. Because we tried to estimate the site amplification factors under similar conditions for the Tungurahua and Cotopaxi networks, we limited the total number to 10 at each station. We used 19 total earthquakes to obtain the site amplification factors for the Tungurahua network, because of the difficulty in obtaining seismograms of an earthquake recorded at all the stations.

[20] We applied band-pass filters in five bands (1–6, 3–8, 5–10, 7–12, and 9–14 Hz) to observed velocity vertical waveforms of the tectonic earthquakes and estimated the envelopes of the band-passed waveforms. In each waveform we used five windows, each of which had a 10 s interval and

a 5 s overlap starting from a lapse time that was twice the S -wave arrival time, and we averaged the mean amplitudes in individual windows. The estimated ratios of BNAS/BVC2 at Cotopaxi and those of BMAS/BRUN at Tungurahua are shown in Figures 3a and 3b, respectively. Although these ratios display scatter, these results show that the ratios increase with increasing frequency. The estimated site amplification factors for all the stations are listed in Table 1.

4.2. A Very-Long-Period (VLP)/LP Event at Cotopaxi

[21] We first applied the waveform inversion and source location methods to a VLP event accompanying LP signals at Cotopaxi on 14 January 2009 that was observed by the five broadband seismic stations. Broadband and band-passed (5–12.5 s) vertical velocity waveforms of the event are shown in Figure 4. An amplitude spectrum of the vertical velocity waveform at BREF is plotted in Figure 5. The event displayed impulsive VLP signals at event onset (Figure 4) that were accompanied by LP signals having broad spectral peaks between 1 and 15 Hz (Figure 5). Similar events showing VLP/LP signals have been observed at Cotopaxi

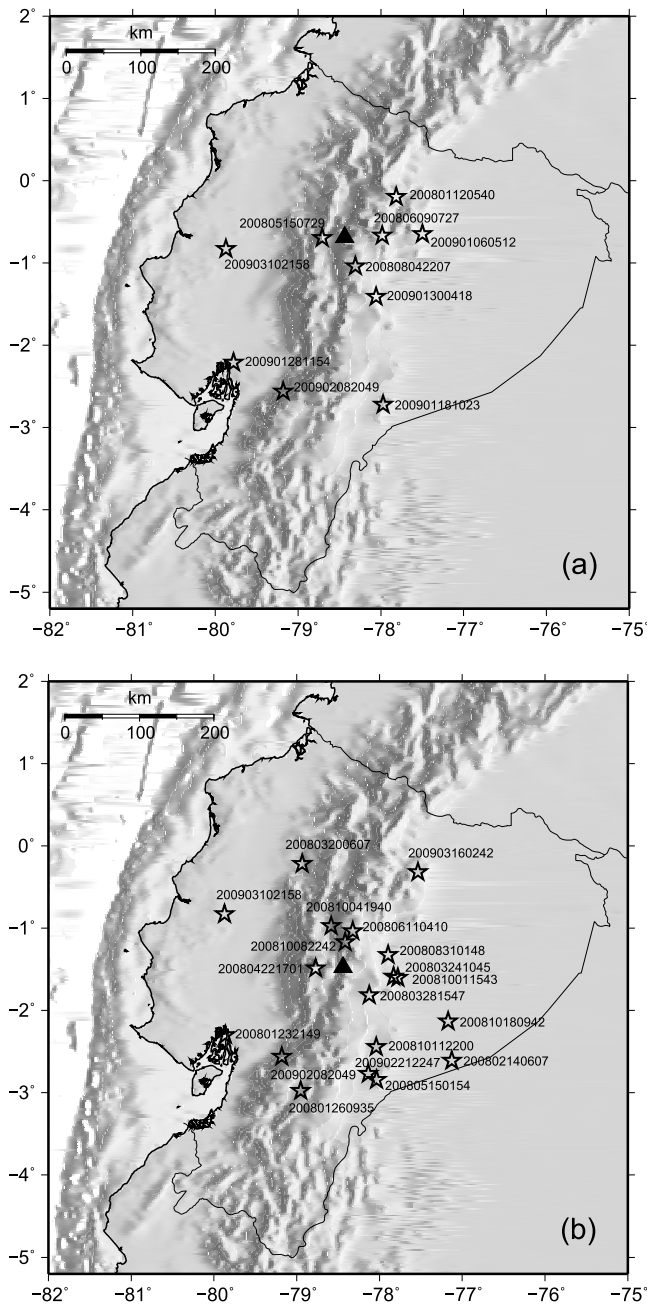


Figure 2. Locations of tectonic earthquakes used to estimate site amplification factors for the stations at (a) Cotopaxi and (b) Tungurahua. Open stars and numbers indicate the locations and source origin times of tectonic earthquakes, respectively. Filled triangles are the locations of (a) Cotopaxi and (b) Tungurahua.

from late June 2002 and were interpreted as the signals generated by gas-release processes in an intruded dike beneath Cotopaxi [Molina et al., 2008].

[22] We performed the waveform inversion of the VLP signals of the VLP/LP event. We used Green’s functions calculated with Domain 1 ($20 \times 20 \times 20$ km) by using the topography of Cotopaxi and assuming a homogeneous medium with P -wave velocity (α) of 3500 m/s, S -wave velocity (β) of 2000 m/s, and density (ρ) of 2650 kg/m³

[Molina et al., 2008]. We applied a band-pass filter between 5 and 12.5 s to the observed three-component displacement seismograms, then decimated them to a sampling interval of 0.12 s.

[23] We assumed isotropic and crack mechanisms in our waveform inversion. As horizontal components at station BNAS were very noisy, we did not use these components. The inversion results (Table 2) indicated that a crack mechanism better explains the observed seismograms. Horizontal and vertical residual distributions obtained from the inversion assuming a crack are plotted in Figure 6a. Waveform fits and the source time function obtained at the best-fit source location are shown in Figure 7. The best-fit source represented by an inclined crack was located at the eastern flank of the volcano (Figure 6a), and the source time function showed a small inflation, followed by a large deflation and subsequent reinflation (Figure 7). These features are consistent with those estimated by Molina et al. [2008] for a VLP/LP event on 26 June 2002. For comparison, residual distributions obtained from the inversion assuming an isotropic mechanism are shown in Figure 6b.

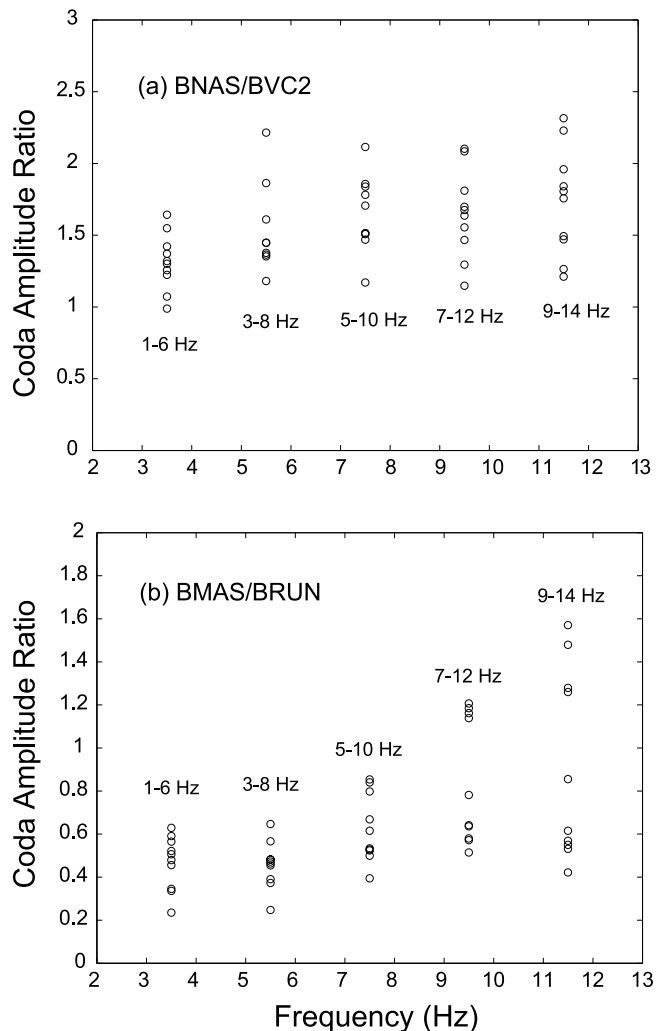


Figure 3. Plots of coda amplitude ratios of (a) BNAS/BVC2 at Cotopaxi and (b) BMAS/BRUN at Tungurahua as a function of frequency.

Table 1. Coda Amplification Factors and Their Standard Deviations in Five Frequency Ranges for the Cotopaxi and Tungurahua Networks, Relative to Stations BVC2 and BRUN, Respectively

| Station | 1–6 Hz | 3–8 Hz | 5–10 Hz | 7–12 Hz | 9–14 Hz |
|-------------------|-------------------|-------------------|-------------------|-------------------|-------------------|
| Cotopaxi | | | | | |
| BVC2 | 1 | 1 | 1 | 1 | 1 |
| BREF | 0.862 ± 0.011 | 0.867 ± 0.010 | 0.962 ± 0.023 | 0.998 ± 0.042 | 1.022 ± 0.133 |
| BNAS | 1.315 ± 0.035 | 1.523 ± 0.083 | 1.647 ± 0.063 | 1.647 ± 0.084 | 1.735 ± 0.127 |
| BMOR | 0.418 ± 0.011 | 0.472 ± 0.012 | 0.589 ± 0.021 | 0.738 ± 0.028 | 1.159 ± 0.062 |
| BTAM | 1.004 ± 0.031 | 1.299 ± 0.052 | 1.575 ± 0.091 | 1.695 ± 0.125 | 1.800 ± 0.193 |
| Tungurahua | | | | | |
| BRUN | 1 | 1 | 1 | 1 | 1 |
| BPAT | 0.487 ± 0.009 | 0.434 ± 0.007 | 0.698 ± 0.020 | 1.021 ± 0.058 | 0.997 ± 0.143 |
| BMAS | 0.466 ± 0.014 | 0.458 ± 0.010 | 0.625 ± 0.023 | 0.842 ± 0.078 | 0.913 ± 0.174 |
| BBIL | 1.015 ± 0.074 | 0.600 ± 0.029 | 0.508 ± 0.027 | 0.626 ± 0.068 | 0.747 ± 0.110 |
| BULB | 0.467 ± 0.022 | 0.363 ± 0.005 | 0.570 ± 0.013 | 0.890 ± 0.066 | 0.960 ± 0.145 |

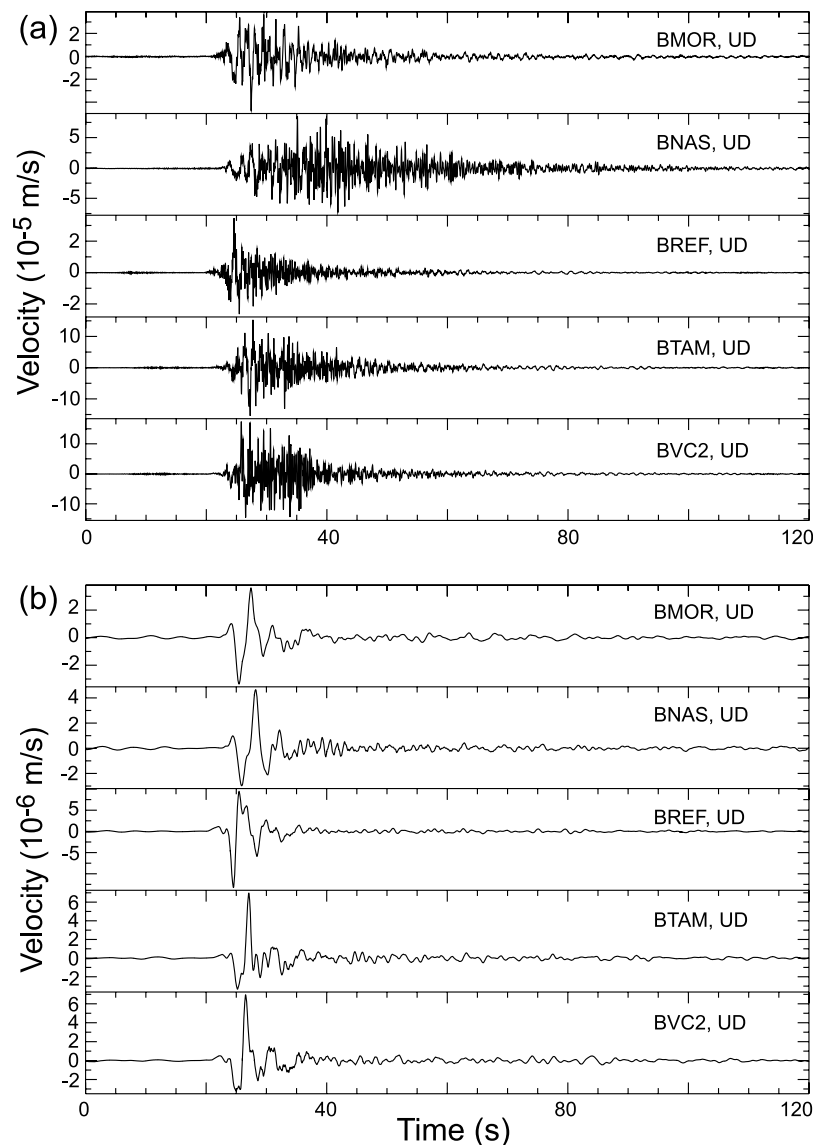


Figure 4. (a) Broadband vertical velocity seismograms of a very-long-period (VLP)/long-period (LP) event observed at Cotopaxi at 1854 on 14 January 2009 (UTC). (b) Waveforms in Figure 4a band-passed between 5 and 12.5 s.

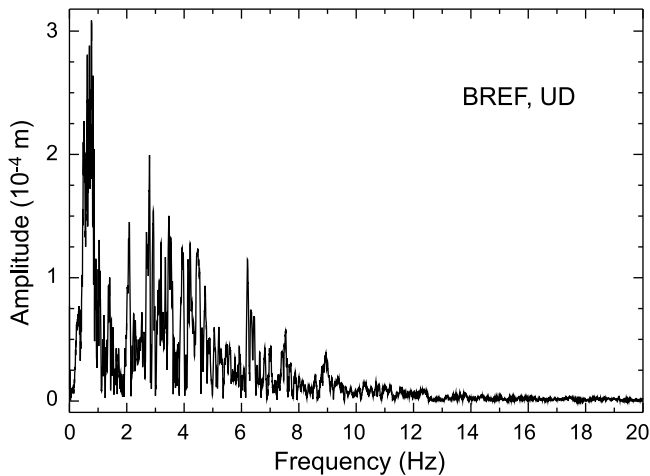


Figure 5. Amplitude spectrum of the vertical velocity seismogram of the VLP/LP event observed at station BREF.

The best-fit source was located at a shallow depth beneath the northern flank, and the residuals were generally higher than those obtained for a crack mechanism. An isotropic mechanism thus may not be appropriate for this VLP/LP event.

[24] We then estimated the source location of the VLP/LP event by using its amplitudes. We applied band-pass filters in five frequency bands (1–6, 3–8, 5–10, 7–12, and 9–14 Hz) to the observed vertical velocity waveforms and obtained the envelopes of the band-passed waveforms. We corrected the envelope amplitudes using the coda amplification factors estimated in the individual frequency bands (Table 1). We used a 30 s time window to estimate the mean amplitude for each waveform. We used $\beta = 2000$ m/s and f as the average of the minimum and maximum frequencies in each frequency band. Figures 8a and 8b show the dependence of the minimum residual locations on the Q factor and frequency band, respectively. In Figure 8a, we used the observed seismograms filtered between 7 and 12 Hz for the spatial grid search using various Q values. In Figure 8b, we used the seismograms in the five frequency bands for the spatial grid search using a fixed Q value of 60. These results indicate that the minimum residual locations display large variations depending on the Q factor and frequency band.

[25] Figure 9a plots the minimum residuals in individual spatial grid searches using the five frequency bands as a function of the Q factor. For comparison, Figure 9b shows the residuals obtained in the same manner as in Figure 9a without the corrections for the site amplification factors. The residuals became smaller in the frequency bands higher than 5 Hz when the seismograms were corrected for the site amplification factors. The residuals in Figure 9a have their global minimum in the frequency band of 7–12 Hz and at $Q = 60$ when corrected for the site amplification factors. Figure 10 shows the spatial distributions of the residuals at individual node points estimated from the spatial grid search using the frequency band of 7–12 Hz and $Q = 60$. The best-fit location was at an elevation of 4 km above sea level beneath the northeastern flank, close to the best-fit location determined by the waveform inversion using the VLP signals (Figure 10). The depths of the two source locations

were the same, and there was a 1-km difference in the north-south direction between the two locations. The difference may be attributed to the limited resolution of both the waveform inversion and the source location results. In view of the residual distributions shown in Figure 10, the depth determined by the source location method was well constrained. This may be because station BREF was located close to and above the source of this event.

4.3. Explosion Event at Tungurahua

[26] We applied the source location method to an explosion event at Tungurahua. Seismic events associated with explosions have been observed frequently at Tungurahua owing to the heightened eruptive activity of this volcano. We used data from an explosion event on 3 May 2009 observed at all five stations in the Tungurahua network (Figure 11). This event was clearly identified as an event associated with an explosion because impulsive acoustic waves were also observed by infrasonic sensors at the individual stations (Figure 11). We note that the explosion event did not produce significant signals in the VLP band. We estimated the source location of the explosion event by using the amplitudes of vertical velocity seismograms, in which we used $\beta = 2000$ m/s and the five frequency bands 1–6, 3–8, 5–10, 7–12, and 9–14 Hz. It is clear in Figure 11 that the seismic records were affected by acoustic waves. Therefore, we used a 10 s time window to use only the initial portions of the seismic signals before the arrivals of acoustic waves.

[27] Figure 12a plots the minimum residuals in individual spatial grid searches using the five frequency bands as a function of the Q factor, in which the seismograms were corrected by the site amplification factors in the individual frequency bands (Table 1). Figure 12b shows the residuals obtained in the same manner as in Figure 12a without the corrections for the site amplification factors. Residuals were smaller when using the seismograms in the frequency bands higher than 5 Hz and without the corrections for the site amplification factors. The global minimum of the residuals in Figure 12 was at the frequency band of 5–10 Hz and $Q = 60$ without the corrections for the site amplification factors. The spatial distributions of the residuals at individual node points estimated from the spatial grid search using the frequency band of 5–10 Hz and $Q = 60$ without the corrections for the site amplification factors are shown in Figure 13. The best-fit source location was close to the active crater on the summit, although the residual pattern is vertically elongated beneath the summit. This vertical elongation is likely due to the lack of a station close to the summit in the Tungurahua network.

Table 2. Inversion Results for the Very-Long-Period/Long-Period Event at Cotopaxi: Normalized Residuals and Corresponding AIC Obtained by the Waveform Inversion Assuming Crack and Isotropic Source Mechanisms^a

| Mechanism | Residual | AIC | (θ , φ) | Location (x , y , z) (km) |
|-----------|----------|-------|--------------------------|-----------------------------------|
| Crack | 0.4196 | -3870 | (30°, 300°) | (0.73, -0.39, 4.00) |
| Isotropic | 0.6018 | -1920 | — | (0.25, 1.05, 4.48) |

^aAIC, Akaike's Information Criterion. Coordinates x , y , and z correspond to east, north, and up from sea level, respectively, and horizontal locations are relative to the summit of Cotopaxi.

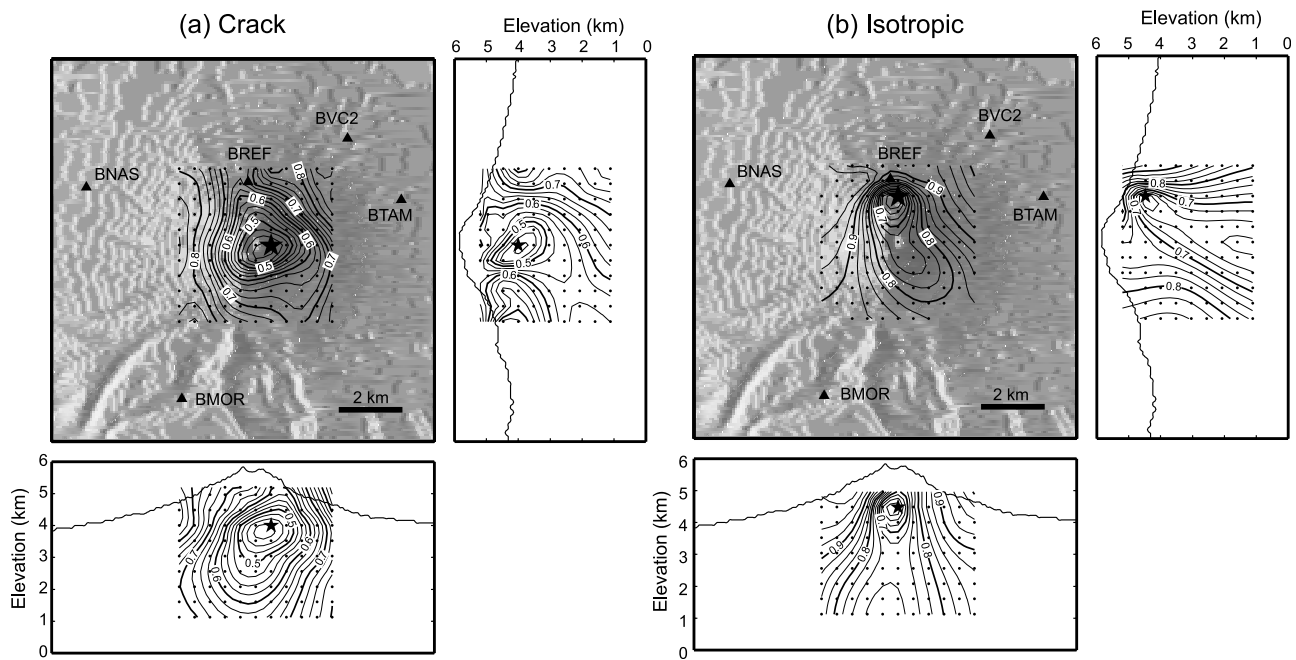


Figure 6. Contour plots of spatial distributions of the normalized residuals obtained by the waveform inversion of the VLP/LP event assuming (a) crack and (b) isotropic mechanisms. Stars show the best-fit locations of the VLP/LP event in the individual inversions. Dots indicates the locations of nodes used in the grid search to estimate the source location.

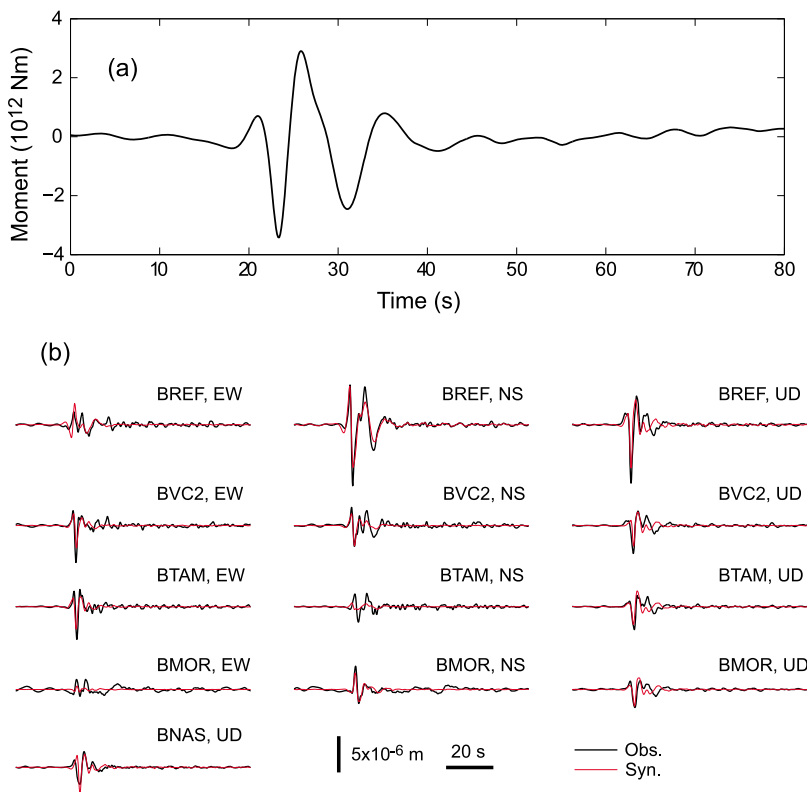


Figure 7. (a) Source time function and (b) waveform match obtained from the waveform inversion of the VLP/LP event assuming a crack. Black and red lines in Figure 7b represent the observed and synthesized seismograms, respectively.

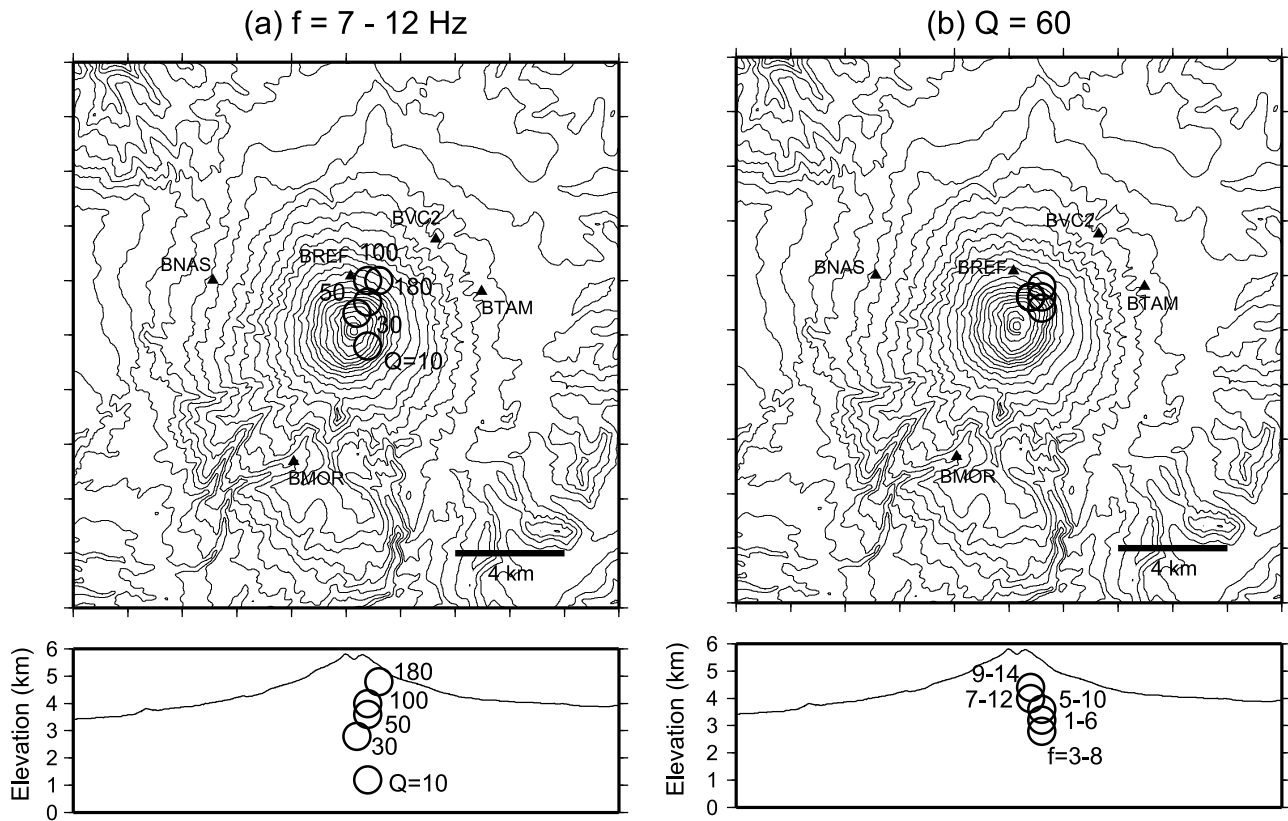


Figure 8. Source locations of the VLP/LP event at Cotopaxi estimated (a) by using amplitudes band-passed between 7 and 12 Hz and assuming various Q values for medium attenuation and (b) by using amplitudes band-passed in five frequency bands (1–6, 3–8, 5–10, 7–12, and 9–14 Hz) and assuming $Q = 60$.

4.4. Tremor Signals Associated with Lahars at Tungurahua

[28] We further applied the source location method to tremor signals associated with lahars that were observed by

the Tungurahua network on 23 August 2008 (Figure 14). A field survey conducted immediately after the tremor occurrence found lahar deposits along the Bascún Valley (Figure 15). As waveform data from station BPAT were not

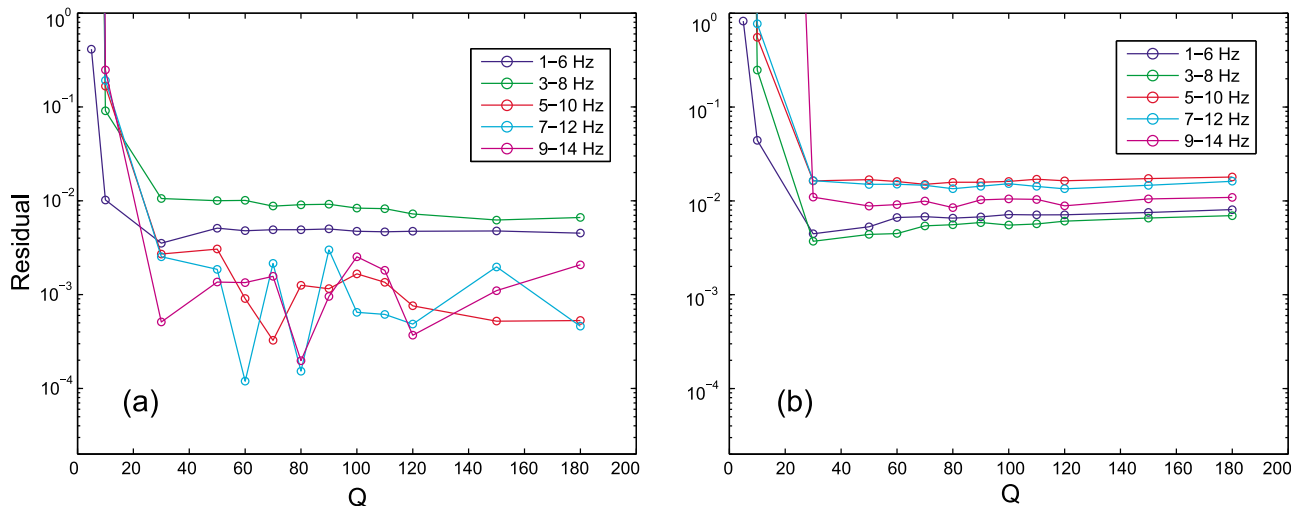


Figure 9. Plots of minimum normalized residuals in individual spatial grid searches for the source location determination of the VLP/LP event at Cotopaxi using amplitudes band-passed in five frequency bands (1–6, 3–8, 5–10, 7–12, and 9–14 Hz) as a function of the Q factor assumed for medium attenuation. The observed amplitudes were (a) corrected by the site amplification factors and (b) uncorrected.

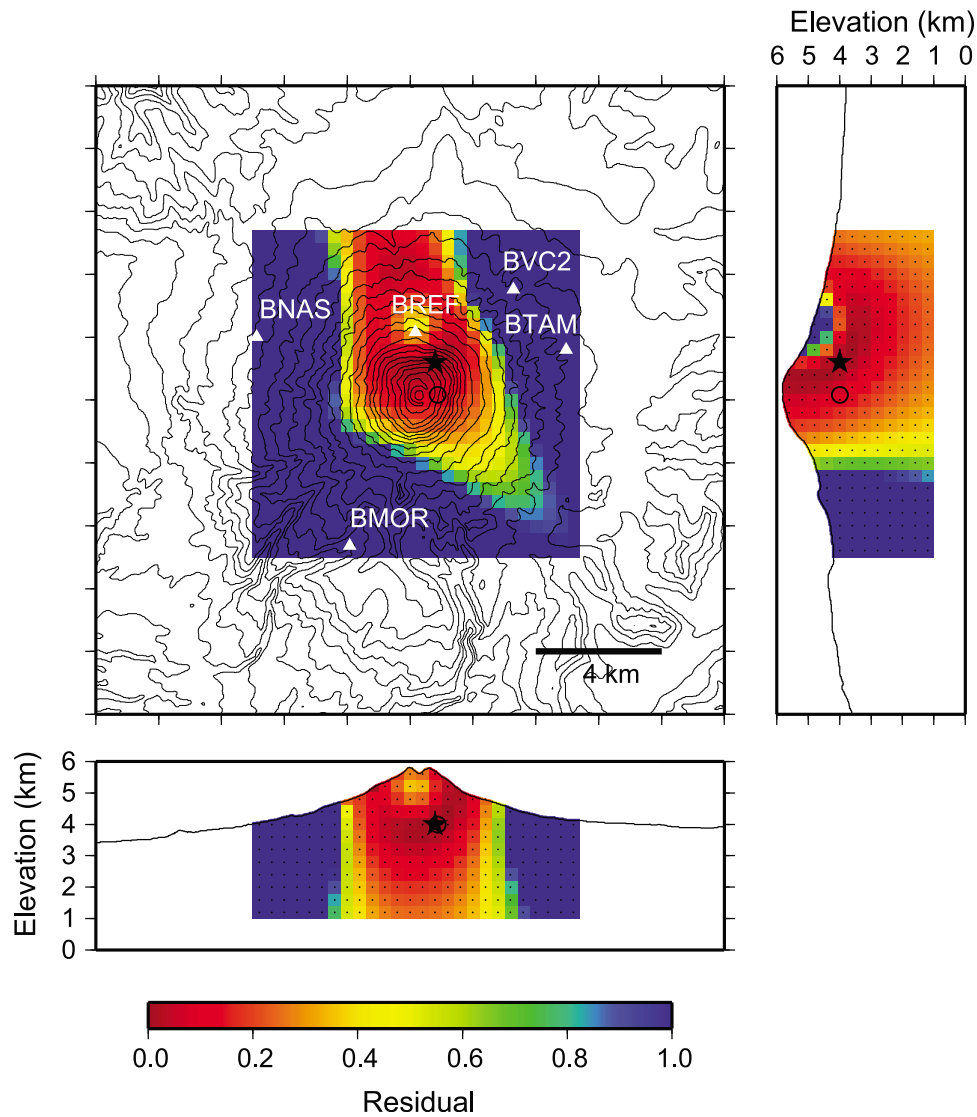


Figure 10. Spatial distributions of the normalized residuals estimated for the VLP/LP event at Cotopaxi using amplitudes band-passed between 7 and 12 Hz and $Q = 60$. Stars indicate the minimum residual point. Circles show the best-fit location obtained from the waveform inversion of the VLP/LP event assuming a crack mechanism. Dots indicate the locations of nodes used in the grid search to estimate the source location.

available because of instrumentation trouble, the tremor signals were observed by four stations. Furthermore, clear signals were only observed at station BRUN, as shown in Figure 14. It is not possible to find the best frequency band and Q factor from the analysis of such signals, so we assume the frequency band of 5–10 Hz and $Q = 60$ without corrections for the site amplification factors, as in the analysis of the explosion event at Tungurahua.

[29] Because P -wave velocity near the surface of Tungurahua was estimated at about 2500 m/s [Molina *et al.*, 2005], we used $\beta = \alpha/\sqrt{3} = 1443$ m/s. We used successive 10 s time windows and node points positioned over the surface of Tungurahua in our spatial grid search. The minimum residual locations in individual time windows plotted in Figure 15 (red stars) indicate that the locations were in the Bascún Valley. For comparison, locations determined by using $Q = 30$ and 100 are also shown in Figure 15 (blue and

green stars, respectively). The locations using $Q = 30$ were west of the valley, and those using $Q = 100$ were the western margin of the valley. These results indicate that the locations using $Q = 60$ in the frequency band of 5–10 Hz were more consistent with field observations.

4.5. VLP and Tremor Signals During a Volcanic Crisis at Tungurahua

[30] We applied the two approaches to seismic signals observed during a volcanic crisis at Tungurahua on 16–17 August 2006. During this crisis, three stations were installed at Tungurahua (Figure 16), of which two (BCUS and Bmas) were damaged by eruptions and associated pyroclastic flows during the crisis (note that Bmas is different from BMAS). Figure 17 displays a 1.5 day long broadband seismic record of the vertical velocity component at station Bmas. This record includes tremor signals of

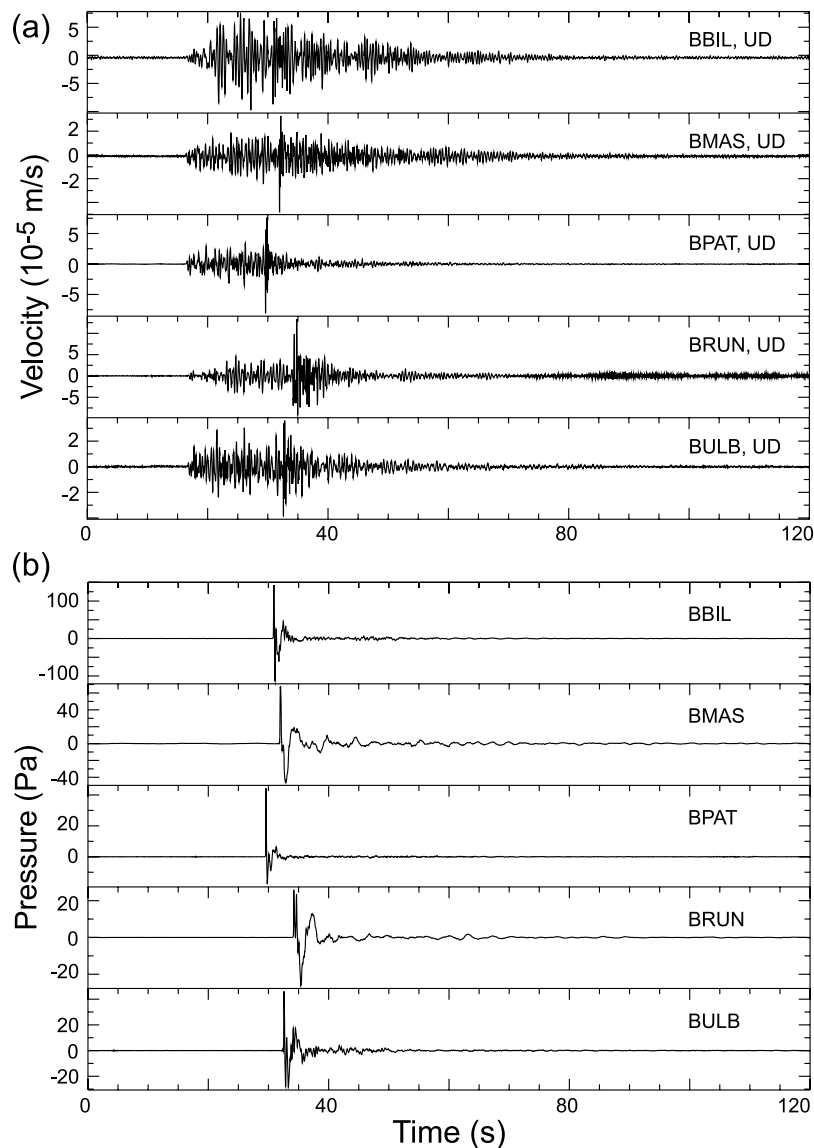


Figure 11. Vertical velocity seismograms (a) and infrasonic records (b) of an explosion event observed at Tungurahua at 1131 on 3 May 2009 (UTC).

gradually increasing amplitude after 1300 on 16 August. A series of vulcanian eruptions accompanied by pyroclastic flows started at 2151 on 16 August. The record of Bmas terminated at about 1750 on 17 August, when the station was damaged. Station BCUS was also damaged at 1425 on 17 August. After the crisis, a survey team from IG-EPN recovered the data loggers kept under the ground at Bmas and BCUS and found them to be undamaged. We used the recovered data for BCUS and Bmas in the following analyses.

[31] Figure 18 shows the records of the vertical velocity components at BCUS, BRUN, and Bmas between 0520 and 0630 on 17 August, for both the broadband seismograms and those band-passed between 10 and 50 s. The broadband seismogram at Bmas shows that tremor amplitudes gradually increased before the time when the station was damaged (arrow), then remained high for 50 min. The feature suggests that the tremor signals were generated by eruptions and pyroclastic flows. The band-passed seismogram at

BCUS shows a noisy sequence, which may reflect local noise originating from eruptions and pyroclastic flows, whereas those from BRUN and Bmas indicate coherent signals before the time of the damage.

[32] We applied the source location method to the tremor signals observed at the three stations, using the frequency range of 5–10 Hz, $Q = 60$, $\beta = 1443$ m/s, successive 10 s time windows, and node points positioned over the surface of Tungurahua. Hereafter, we use a time axis in seconds measured from 1720 on 17 August. In Figure 16 we plot the minimum residual points in individual 10 s time windows during four subdivisions of the tremor records. The estimated source locations of the tremor signals were closer to BCUS in the period between 0 and 1000 s, then moved toward Bmas in the period from 1000 to 2000 s. The tremor sources were located on the southwestern flank between 2000 and 3000 s, and other sources along the northwestern flank, in addition to the southwestern sources, appeared in

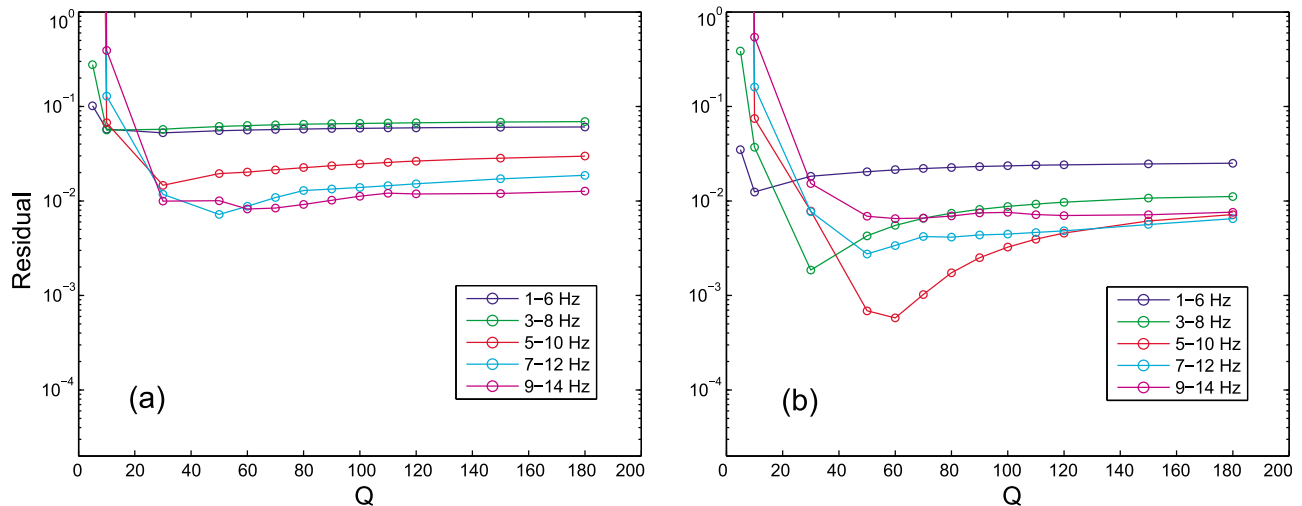


Figure 12. Plots of the minimum normalized residuals in individual spatial grid searches for the source location determination of the explosion event at Tungurahua using amplitudes band-passed in five frequency bands (1–6, 3–8, 5–10, 7–12, and 9–14 Hz) as a function of the Q factor assumed for medium attenuation. The observed amplitudes were (a) corrected by the site amplification factors and (b) uncorrected.

the period from 3000 to 4200 s. These locations matched the distributions of pyroclastic flows and surges estimated by *Barba et al.* [2008] and *Kelfoun et al.* [2009].

[33] We performed the waveform inversion of the VLP signals coherently observed at BRUN and Bmas that are labeled VLP1 and VLP2 in Figure 18b. We applied a band-pass filter between 10 and 50 s to three-component displacement seismograms at the two stations and used Green's functions calculated with domain 2 ($200 \times 200 \times 36$ km) with the topography of Tungurahua and $\alpha = 3500$ m/s, $\beta = 2000$ m/s, and $\rho = 2500$ kg/m³. The inversion results are summarized in Table 3. In both cases an isotropic mechanism better explains the VLP signals than a crack mechanism. Figures 19a and 19b plot the spatial distributions of the residuals obtained from the inversions of VLP1 and VLP2, respectively, assuming an isotropic mechanism. They also show observed and calculated particle motions at individual stations. The best-fit sources (stars in Figures 19a and 19b) were located at depths of 2.1 (VLP1) and 2.4 km (VLP2) above sea level beneath the summit region and explained the observed particle motions fairly well. The difference in the best-fit locations between the two inversion results may be attributed to limited resolution seen as elongations of the residual distributions toward the southwest.

5. Discussion

[34] The source location method obtained the best-fit location of the VLP/LP event at Cotopaxi when using a frequency band of 7–12 Hz and $Q = 60$ (Figure 9). Similarly, this method obtained the best-fit source location of the explosion event at Tungurahua in a frequency band of 5–10 Hz and at $Q = 60$ (Figure 12). These locations may be regarded as reasonable because the location of the VLP/LP event was very close to the best-fit source location estimated from the waveform inversion and the location of the explosion event was determined at a position near the summit crater. These results strongly indicate the existence

of an appropriate frequency band and Q value for the source location determinations using seismic amplitudes. Our interpretation is that the isotropic radiation assumption becomes valid in these bands because of the path effect caused by the scattering of seismic waves propagating in structural heterogeneities beneath the volcanoes. The waveform inversion of the VLP/LP event at Cotopaxi indicates that a crack mechanism is preferable to an isotropic mechanism, suggesting that isotropic radiation is not inherent to the source but is caused by the path effect. Our results are therefore in good agreement with those from the studies of tectonic earthquakes by *Liu and Helmberger* [1985] and *Takemura et al.* [2009]. Although for this interpretation the isotropic radiation assumption may be valid at frequencies higher than 5 Hz, noise becomes dominant in frequency bands higher than 10–12 Hz. Whereas *Battaglia and Aki* [2003] noted that the Q factor does not have a large influence on the location of events, our study indicates that the location depends largely on the Q factor (Figure 8), and a Q factor of about 60 provided the best-fit locations for both the VLP/LP event at Cotopaxi and the explosion event at Tungurahua. This value of Q is close to the value $Q = 50$ used by *Battaglia and Aki* [2003].

[35] We also showed that the source location method using the frequency band of 5–10 Hz and $Q = 60$ provided the reasonable source locations for the tremor signals associated with lahars and pyroclastic flows at Tungurahua. These results further support the appropriateness of the use of the frequency band and Q value. *Kumagai et al.* [2009] used a frequency band of 1–3 Hz to locate sources of tremor signals associated with lahars, assuming that the tremor signals were dominantly excited by surface waves in this band. We also used the 1–3 Hz frequency band, assuming an amplitude decrease of $1/\sqrt{r}$ instead of $1/r$ in equation (8), for the tremor signals associated with lahars at Tungurahua. We found that the source locations also lay beneath Bascún Valley if we used a value of Q of about 30. This frequency band and the assumption of the surface wave

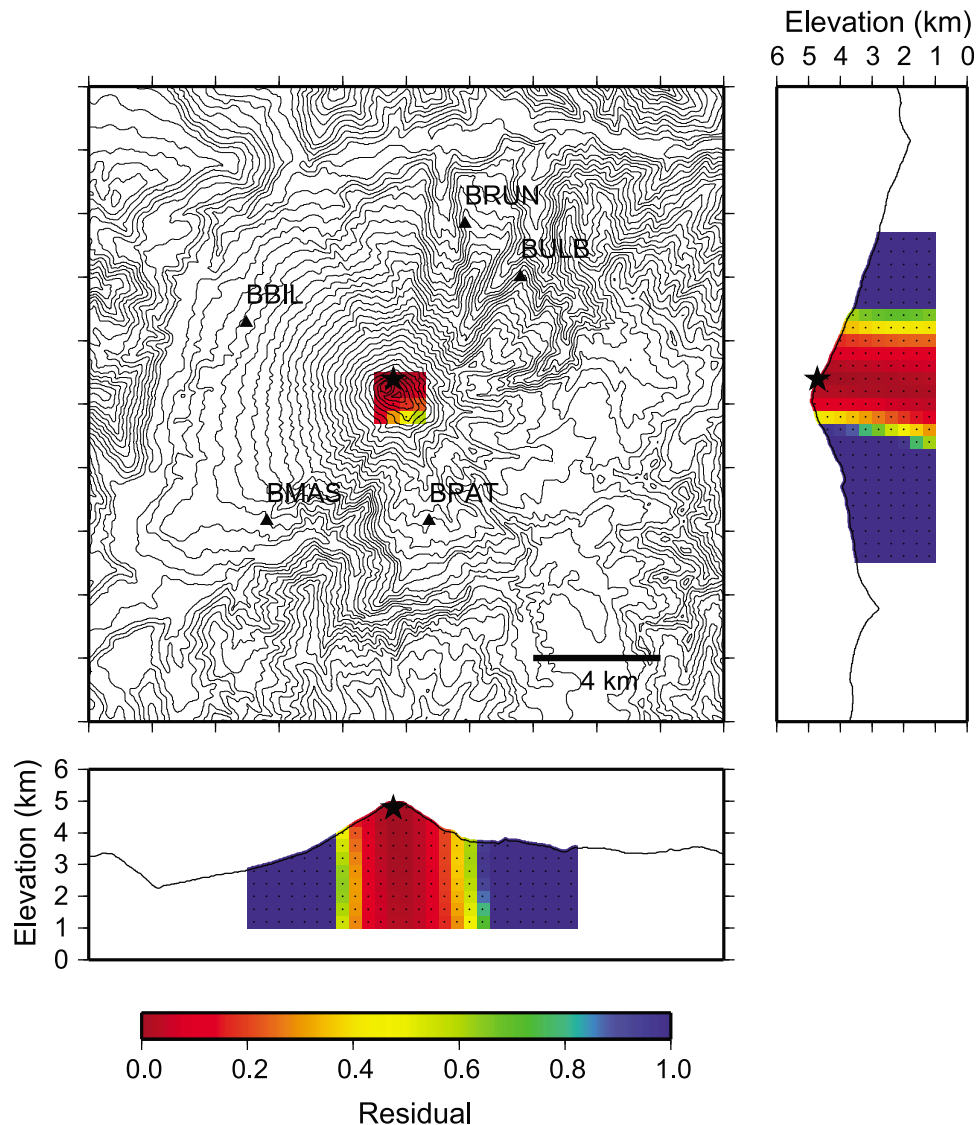


Figure 13. Spatial distributions of the normalized residuals estimated for the explosion event at Tungurahua using amplitudes band-passed between 5 and 10 Hz and $Q = 60$. Stars indicate the minimum residual point. Dots indicate the locations of nodes used in the grid search to estimate the source location.

excitation may also be appropriate for tremor signals originating from lahars and pyroclastic flows. However, given that the frequency band 5–12 Hz and a Q of about 60 provide successful results for various seismic events and tremor signals, the use of these values may be more systematic.

[36] We assumed S -wave amplitudes for our source location determinations. *Matsumoto and Hasegawa* [1991] suggested that there is a large contribution from converted S waves derived from P waves in seismograms recorded in a volcanic area observing a marine air gun source, which may radiate purely isotropic P waves. *Aki* [1992] theoretically showed that P - S conversion scattering occurs more readily than S - P conversion scattering, suggesting that S waves dominate over P waves in the coda. As shown by *Wegler and Lühr* [2001] and *Wegler* [2003] from active seismic experiments at volcanoes, there are strong scattering effects in volcanic environments. Therefore, seismic waves observed at volcanoes may be dominated by S waves, especially in a

high-frequency range even for explosion events, which may have isotropic mechanisms. To check this point, we also used P -wave velocity ($\alpha = 3500$ m/s) in the source location determination of the explosion event at Tungurahua. In that case the global minimum residual was an order of magnitude larger than the one obtained using S -wave velocity, which also supports our assumption.

[37] The site amplification factors we estimated for the Cotopaxi network improved the fits to the observed amplitudes of the VLP/LP event. On the contrary, the site amplification factors for the Tungurahua network worsened the fits for the explosion event at Tungurahua. Because Tungurahua was actively erupting, there was probably a clear magmatic system beneath the volcano. In such a system seismic scatterers may not be uniformly distributed, which violates the basic assumption for the coda normalization method that the seismic energy is uniformly distributed in the volume surrounding the source and stations.

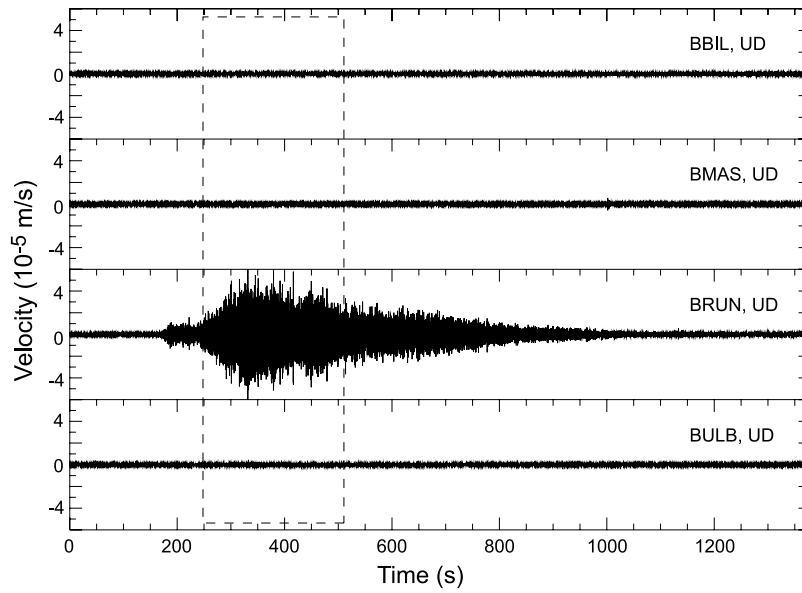


Figure 14. Vertical velocity tremor signals associated with lahars at Tungurahua. Time in seconds along the horizontal axis starts from 0453:00 on 23August 2008 (UTC). Signals enclosed by the dashed rectangle are used in Figure 15.

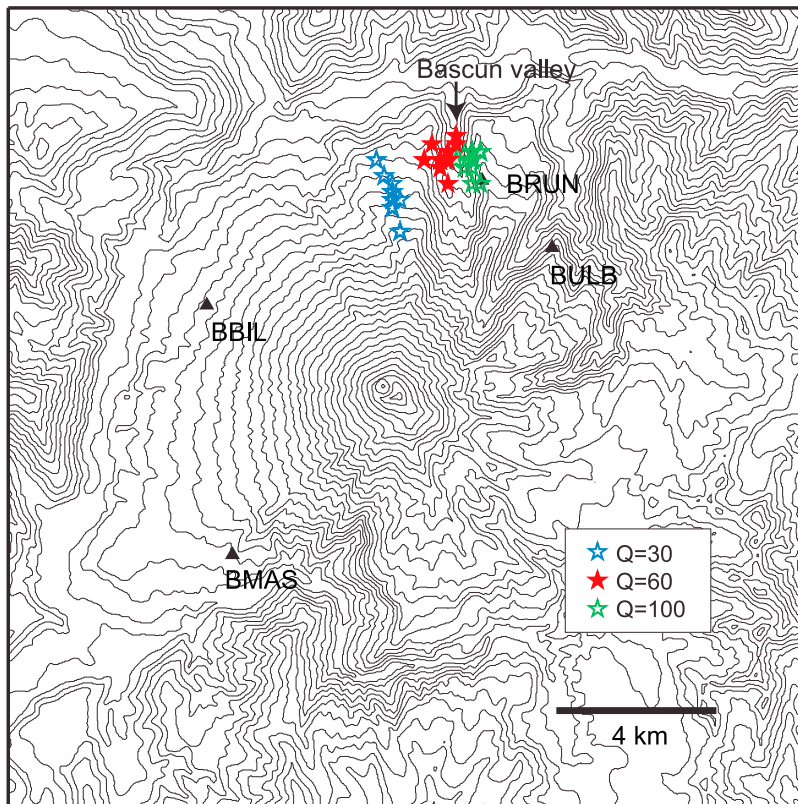


Figure 15. Source locations of the tremor signals in the selected data in Figure 14. Red, blue, and green stars indicate the minimum residual locations of the tremor signals estimated by using the amplitudes band-passed between 5 and 10 Hz and assuming $Q = 60, 30,$ and $100,$ respectively, in individual 10 s windows.

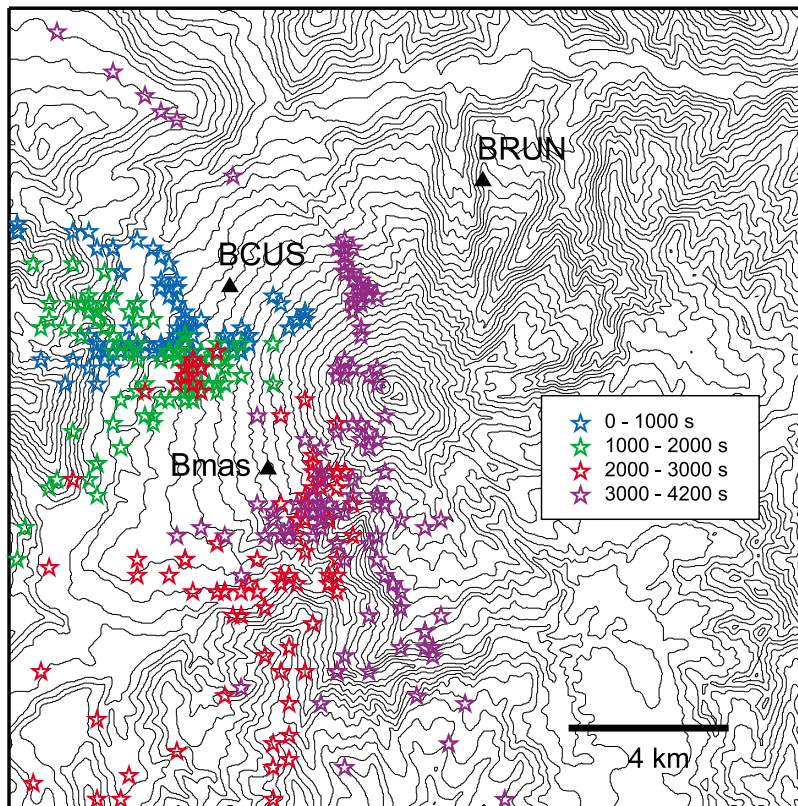


Figure 16. Locations of broadband seismic and infrasonic stations at Tungurahua during the volcanic crisis of 16–17 August 2006 and the source locations of the tremor signals in Figure 18. Blue, green, red, and purple stars indicate the minimum residual positions of the tremor signals estimated by using the amplitudes band-passed between 5 and 10 Hz and $Q = 60$ in individual 10 s windows during the time intervals of 0–1000, 1000–2000, 2000–3000, and 3000–4200 s, respectively, on the time axis shown in Figure 18.

Furthermore, the explosion event was a shallow source and had strong seismic energy near the surface of the volcano. Thus, the paths from this source to the stations differed from those used in deriving the site amplification factors, which may also result in different scattering effects. At Cotopaxi, the source of the VLP/LP event was beneath the Cotopaxi network and the magma system may not have been maturely developed given that this volcano was not erupting. These conditions may account for the successful use of the site amplification factors for the Cotopaxi network.

[38] Our waveform inversion of the VLP signals during the volcanic crisis of Tungurahua indicated that the sources were at depths of 2.1–2.4 km above sea level or 2.6–2.9 km beneath the summit (Figure 19). The VLP signals were better explained by an isotropic mechanism than a crack mechanism (Table 3), although the difference in AIC was small, especially for VLP1 (Table 3). The VLP sources were thus constrained by using the waveform data from only two stations, although the resolutions were limited. This feature is consistent with the synthetic tests of *Nakano and Kumagai* [2005], which showed that waveform data from 2 to 3 three-component stations can estimate the source mechanism and location in this waveform inversion approach. The VLP sources characterized by volumetric changes beneath

the summit region strongly suggest that these signals had a magmatic origin. VLP signals associated with eruptions have been observed at Popocatepetl, México [*Chouet et al.*, 2005], and Mount St. Helens, Washington, USA [*Waite et al.*, 2008], and their sources were also characterized by volumetric changes, which have been interpreted to be the result of degassing processes in magma. The VLP signals at Tungurahua also may have been generated by degassing in magma entering a conduit at these depths beneath the summit. To explore this interpretation, we estimated the mass fraction of water (n_w) dissolved in an andesitic magma from Tungurahua under saturation conditions at a depth of 2.6 km as follows. Using Henry's law [e.g., *Sparks*, 1978] and assuming a closed conduit (lithostatic pressure, 65 MPa) and Henry's constant = 9×10^{-12} to 1.6×10^{-11} Pa $^{-1}$ [*Nishimura*, 2004], we obtained $n_w = 2.4$ –3.2 wt%. The Tungurahua magma, therefore, may initially contain at least 2.4–3.2 wt% water for degassing to occur at this depth. Amphiboles are the phase most indicative of volatile abundance, but they are not found in recent volcanic products from Tungurahua, suggesting that the water content of the magma is less than 3–4 wt% [*Cashman*, 2004]. This is consistent with our interpretation that the VLP signals were generated by volumetric changes associated with bubble

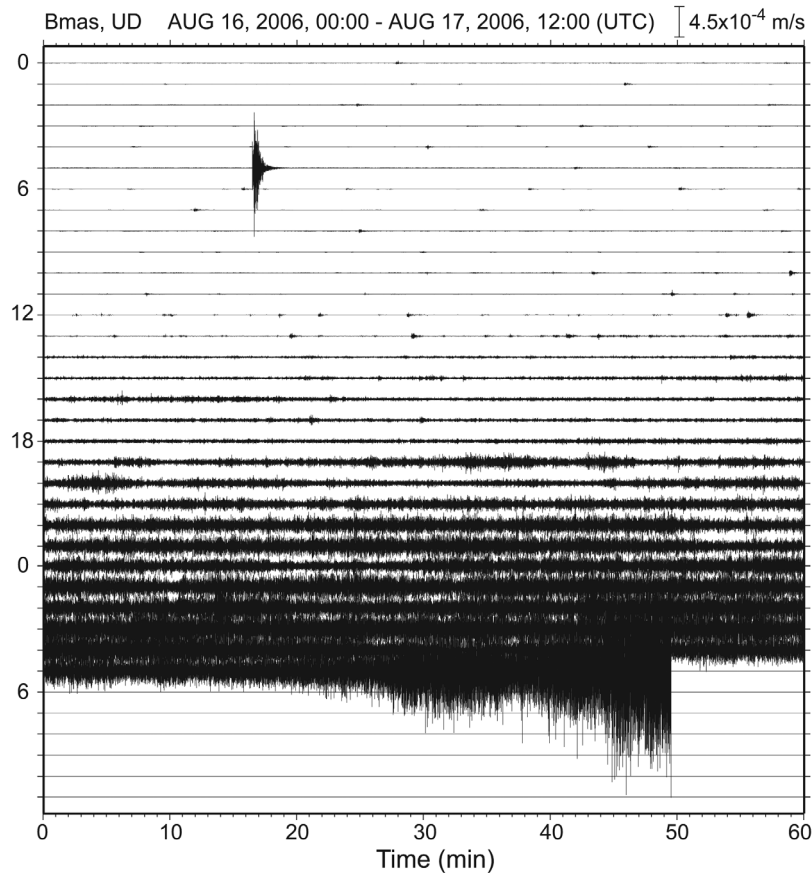


Figure 17. A 1.5 day long broadband seismic record of the vertical velocity component at station Bmas. The record terminated at about 1750 on 17 August 2006 (UTC), when the station was damaged by the eruption and its associated pyroclastic flows.

growth in magma. As a result of bubble growth, the magma became more buoyant and ascended more rapidly in the conduit. A rapid magma ascent may have produced the vulcanian eruptions with accompanying pyroclastic flows that damaged station Bmas. If the VLP signals are a precursor of explosive eruptions, then monitoring them is particularly important.

[39] As demonstrated above, the source location and waveform inversion methods are useful to analyze various volcano-seismic signals. Our results suggest that the source location method may be valid for frequencies higher than 5 Hz, where S waves show an isotropic radiation pattern due to the path effect caused by the scattering of seismic waves. Therefore, this method may be categorized as a stochastic approach based on the nature of scattering waves. The waveform inversion, which is a purely deterministic approach, is applicable to waveform data from a few stations but only in periods longer than a few seconds. Volcano-seismic signals around 1 s remain problematic, because signals in this band may have both stochastic and deterministic characters. These features in different periods are quite consistent with the classification of scattering problems and applicable methods in the ka-kL diagram proposed by *Aki and Richards* [1980]. The waveform inversion in the frequency domain assuming a crack and using a spatial grid search with an adaptive grid spacing enabled us

to find a solution within 3–4 min using a personal computer (Intel Xeon; 3 GHz) with a Linux operating system. The waveform inversion assuming an isotropic source was much faster, yielding a solution within 1 min. The source location method also provided a final solution within 1 min. Therefore, if multiple CPUs are available, we can perform the waveform inversion and the source location determination simultaneously to estimate source parameters of various volcano-seismic signals in almost real time.

6. Conclusions

[40] We systematically used two approaches to analyze broadband seismic signals observed at active volcanoes: a source location method of LP events and tremor using their amplitudes and a waveform inversion of VLP signals in the frequency domain assuming possible source mechanisms. The source location method assumes isotropic wave radiation, which is apparently inconsistent with the hypothesis of a crack geometry at the LP source. However, the isotropic radiation assumption may be valid in a high-frequency range in which the path effect caused by the scattering of seismic waves results in an isotropic radiation pattern of S waves. Using this method, we estimated the best-fit source location of a VLP/LP event at Cotopaxi using a frequency band of 7–12 Hz and $Q = 60$. This location was close to the

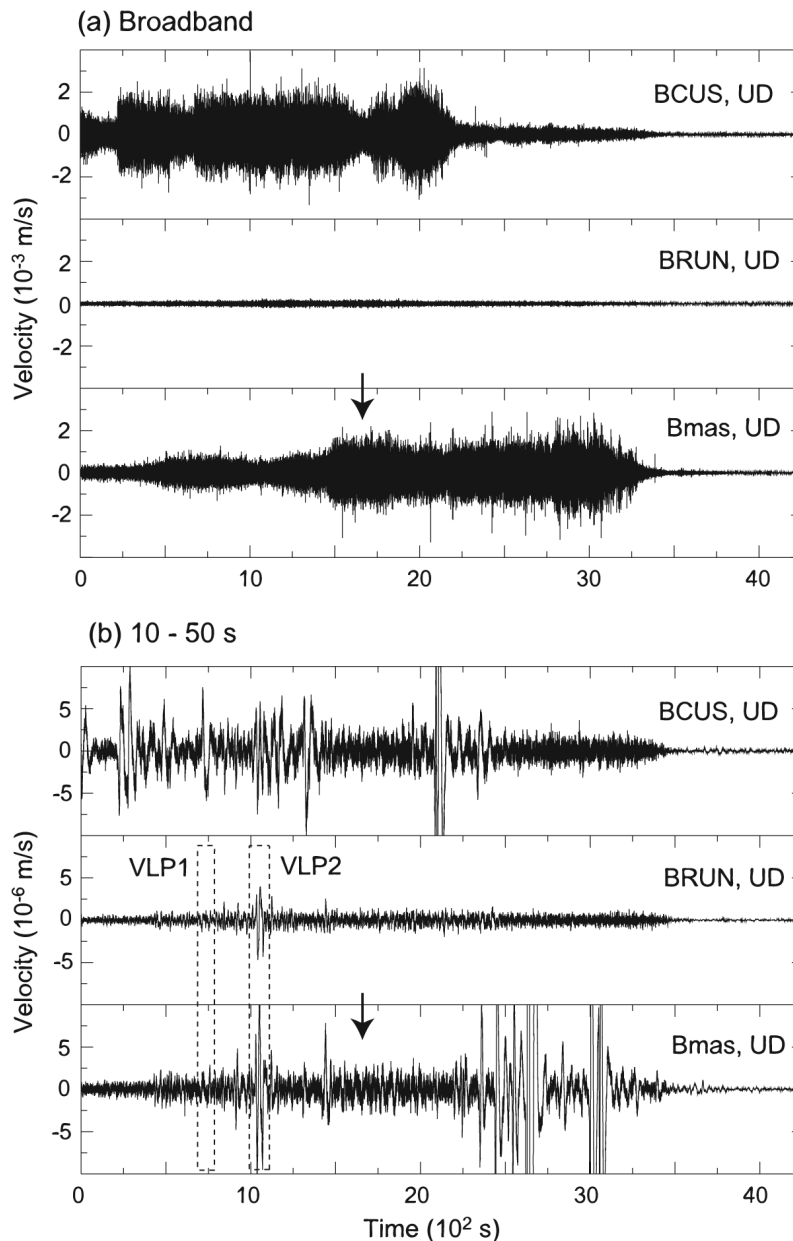


Figure 18. Broadband vertical waveforms (a) and band-passed (10–50 s) vertical waveforms (b) observed at stations BCUS, BRUN, and Bmas between 1720 and 1830 on 17 August 2006 (UTC). Arrows indicate the time at which the station Bmas was damaged. VLP signals in the rectangular outlines in Figure 18b (VLP1 and VLP2) are used in Figure 19.

best-fit source location determined by waveform inversion of the VLP/LP event using a VLP band of 5–12.5 s. The waveform inversion indicated that a crack mechanism better explained the VLP signals than an isotropic mechanism. These results support our interpretation that isotropic radiation is not inherent to the source and only appears at high frequencies. We also obtained a best-fit location of an explosion event at Tungurahua when using a frequency band of 5–10 Hz and $Q = 60$. This result also supports our interpretation of isotropic radiation and suggests that a frequency band around 5–12 Hz and a Q factor of about 60 are appropriate for determining source locations. This

frequency band and Q value also yielded reasonable locations for the sources of tremor signals associated with lahars and pyroclastic flows at Tungurahua. We applied the waveform inversion to VLP signals observed at only two stations during a volcanic crisis of Tungurahua. We determined best-fit source locations at depths of 2.6–2.9 km beneath the summit region, and these sources were consistently explained by volumetric changes caused by bubble growth in magma. The stochastic approach of the source location method and the deterministic approach based on the waveform inversion both are useful to better utilize broadband seismic signals observed at a limited number of sta-

Table 3. Inversion Results for the VLP signals (VLP1 and VLP2) at Tungurahua: Normalized Residuals and Corresponding AIC Obtained by the Waveform Inversion Assuming Crack and Isotropic Source Mechanisms^a

| Event | Mechanism | Residual | AIC | (θ , φ) | Location (x , y , z) (km) |
|-------|-----------|----------|-------|--------------------------|--------------------------------------|
| VLP1 | Crack | 0.1993 | -1055 | (60°, 40°) | (-1.3, -1.0, 2.4) |
| | Isotropic | 0.1992 | -1060 | — | (-0.7, -0.4, 2.1) |
| VLP2 | Crack | 0.1275 | -1809 | (80°, 260°) | (-1.0, -0.4, 2.1) |
| | Isotropic | 0.1263 | -1823 | — | (-0.7, 0.2, 2.4) |

^aAIC, Akaike's Information Criterion; VLP, very long period. Coordinates x , y , and z correspond to east, north, and up from sea level, respectively, and horizontal locations are relative to the summit of Tungurahua.

tions at active volcanoes and contribute to improved seismic volcano monitoring.

Appendix A: Source Location Determination Using Seismic Amplitudes

[41] We use equations (8) and (9), in which we assume S -wave amplitude. We assume that \dot{s} in equation (8) is represented by the δ function in the following form:

$$\dot{s}(t) = s_0 \delta(t - t_s), \quad (\text{A1})$$

where t_s is the source origin time. Then equation (8) is rewritten as

$$u_i(t + r_i/\beta) = A'_0 \frac{e^{-Br}}{r_i} \delta(t - t_s), \quad (\text{A2})$$

where $A'_0 = A_0 s_0$. We use equation (A2) to fit observed amplitudes by minimizing the normalized residual E defined as

$$E = \frac{\sum_{i=1}^N \{u_i^o(t_s + r_i/\beta) - u_i(t_s + r_i/\beta)\}^2}{\sum_{i=1}^N \{u_i^o(t_s + r_i/\beta)\}^2}, \quad (\text{A3})$$

where N is the number of stations and u_i^o is the observed amplitude at the i th station. Minimizing E leads to the following solution at $t = t_s$:

$$A'_0 = \frac{1}{N} \sum_{i=1}^N u_i^o(t_s + r_i/\beta) r_i e^{Br_i}. \quad (\text{A4})$$

We perform a spatial grid search in each origin time t_s to find the best-fit source location. The amplitude u_i^o is averaged over a time window in each observed waveform. We assume the δ function for \dot{s} , implying that the source duration is assumed to be short compared to the time window. If multiple sources exist in a time window, this method may not provide correct source locations [e.g., Kumagai *et al.*, 2009].

Appendix B: Waveform Inversion in the Frequency Domain

[42] The displacement field in equation (1) is written in the frequency domain in a discrete form as follows:

$$\bar{u}_i(k\Delta\omega) = \sum_{j=1}^6 \bar{m}_j(k\Delta\omega) \bar{G}_{ij}(k\Delta\omega), \quad (\text{B1})$$

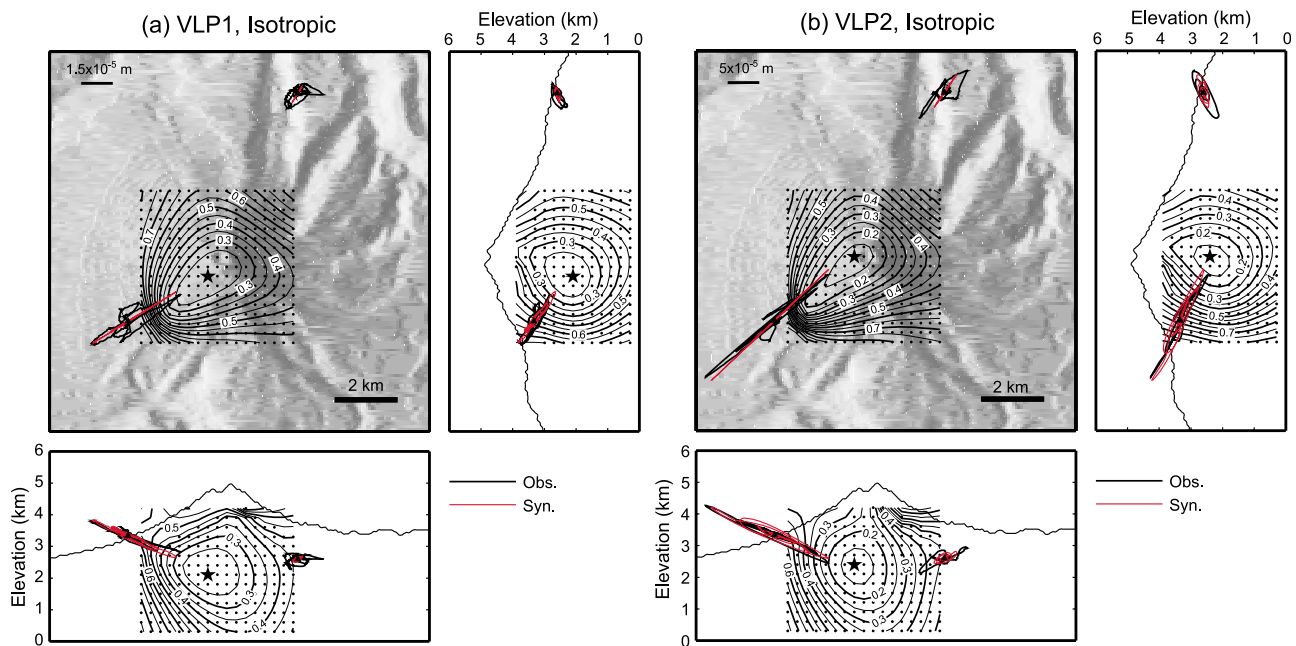


Figure 19. Contour plots of spatial distributions of the normalized residuals obtained by the waveform inversions of (a) VLP1 and (b) VLP2 (Figure 18b) assuming an isotropic mechanism. Stars show the best-fit locations in the individual inversions. Observed (black lines) and synthetic (red lines) particle motions obtained from displacement seismograms are also plotted. Dots indicate the locations of nodes used in the grid searches to estimate the source locations.

- IASPEI International Handbook of Earthquake and Engineering Seismology*, edited by W. H. K. Lee et al., Academic, London.
- Kaneshima, S., et al. (1996), Mechanism of phreatic eruptions at Aso volcano inferred from near-field broadband seismic observations, *Science*, *273*, 642–645, doi:10.1126/science.273.5275.642.
- Kawakatsu, H., and M. Yamamoto (2007), Volcano seismology, in *Treatise on Geophysics*, vol. 4, edited by H. Kanamori, pp. 389–420, Elsevier, Amsterdam, doi:10.1016/B978-0-444-52748-6.00073-0.
- Kawakatsu, H., T. Ohminato, H. Ito, Y. Kuwahara, T. Kato, K. Tsuruga, S. Honda, and K. Yomogida (1992), Broadband seismic observation at Sakurajima Volcano, Japan, *Geophys. Res. Lett.*, *19*(19), 1959–1962, doi:10.1029/92GL01964.
- Kawakatsu, H., T. Ohminato, and H. Ito (1994), 10s-period volcanic tremors observed over a wide area in southwestern Japan, *Geophys. Res. Lett.*, *21*(18), 1963–1966, doi:10.1029/94GL01683.
- Kawakatsu, H., S. Kaneshima, H. Matsubayashi, T. Ohminato, Y. Sudo, T. Tsutsui, K. Uhira, H. Yamasato, H. Ito, and D. Legrand (2000), Aso94: Aso seismic observation with broadband instruments, *J. Volcanol. Geotherm. Res.*, *101*, 129–154, doi:10.1016/S0377-0273(00)00166-9.
- Kelfoun, K., P. Samaniego, P. Palacios, and D. Barba (2009), Testing the suitability of frictional behavior for pyroclastic flow simulation by comparison with a well-constrained eruption at Tungurahua volcano (Ecuador), *Bull. Volcanol.*, *71*, 1057–1075, doi:10.1007/s00445-009-0286-6.
- Kobayashi, T., T. Ohminato, Y. Ida, and E. Fujita (2009), Very long period seismic signals observed before the caldera formation with the 2000 Miyake-jima volcanic activity, Japan, *J. Geophys. Res.*, *114*, B02211, doi:10.1029/2007JB005557.
- Kumagai, H., T. Ohminato, M. Nakano, M. Ooi, A. Kubo, H. Inoue, and J. Oikawa (2001), Very-long-period seismic signals and caldera formation at Miyake Island, Japan, *Science*, *293*, 687–690, doi:10.1126/science.1062136.
- Kumagai, H., B. A. Chouet, and M. Nakano (2002), Waveform inversion of oscillatory signature in long-period events beneath volcanoes, *J. Geophys. Res.*, *107*(B11), 2301, doi:10.1029/2001JB001704.
- Kumagai, H., K. Miyakawa, H. Negishi, H. Inoue, K. Obara, and D. Suetsugu (2003), Magmatic dike resonances inferred from very-long-period seismic signals, *Science*, *299*, 2058–2061, doi:10.1126/science.1081195.
- Kumagai, H., B. A. Chouet, and P. B. Dawson (2005), Source process of a long-period event at Kilauea volcano, Hawaii, *Geophys. J. Int.*, *161*, 243–254, doi:10.1111/j.1365-246X.2005.02502.x.
- Kumagai, H., et al. (2007), Enhancing volcano-monitoring capabilities in Ecuador, *Eos Trans. AGU*, *88*, 245–246, doi:10.1029/2007EO230001.
- Kumagai, H., P. Palacios, T. Maeda, D. Barba Castillo, and M. Nakano (2009), Seismic tracking of lahars using tremor signals, *J. Volcanol. Geotherm. Res.*, *183*, 112–121, doi:10.1016/j.jvolgeores.2009.03.010.
- Legrand, D., S. Kaneshima, and H. Kawakatsu (2000), Moment tensor analysis of near-field broadband waveforms observed at Aso Volcano, Japan, *J. Volcanol. Geotherm. Res.*, *101*, 155–169, doi:10.1016/S0377-0273(00)00167-0.
- Liu, H.-L., and D. V. Helmberger (1985), The 23:19 aftershock of the 15 October 1979 Imperial Valley earthquake: More evidence for an asperity, *Bull. Seismol. Soc. Am.*, *75*, 689–708.
- Lockmer, I., C. J. Bean, G. Saccorotti, and D. Patanè (2007), Moment-tensor inversion of LP events recorded on Etna in 2004 using constraints obtained from wave simulation tests, *Geophys. Res. Lett.*, *34*, L22316, doi:10.1029/2007GL031902.
- Matsumoto, S., and A. Hasegawa (1991), Estimation of relative site effect, coda Q and scattering strength from the records obtained by a large airgun experiment, *Phys. Earth Planet. Inter.*, *67*, 95–103, doi:10.1016/0031-9201(91)90063-N.
- Mayeda, K., S. Koyanagi, and K. Aki (1991), Site amplification from S-wave coda in the Long Valley caldera region, California, *Bull. Seismol. Soc. Am.*, *81*, 2194–2213.
- Molina, I., H. Kumagai, J.-L. Le Pennec, and M. Hall (2005), Three-dimensional P wave velocity structure of Tungurahua Volcano, Ecuador, *J. Volcanol. Geotherm. Res.*, *147*, 144–156, doi:10.1016/j.jvolgeores.2005.03.011.
- Molina, I., H. Kumagai, A. García-Aristizábal, M. Nakano, and P. Mothes (2008), Source process of very-long-period events accompanying long-period signals at Cotopaxi Volcano, Ecuador, *J. Volcanol. Geotherm. Res.*, *176*, 119–133, doi:10.1016/j.jvolgeores.2007.07.019.
- Nakano, M., and H. Kumagai (2005), Waveform inversion of volcano-seismic signals assuming possible source geometries, *Geophys. Res. Lett.*, *32*, L12302, doi:10.1029/2005GL022666.
- Nakano, M., H. Kumagai, and B. A. Chouet (2003), Source mechanism of long-period events at Kusatsu-Shirane Volcano, Japan, inferred from waveform inversion of the effective excitation functions, *J. Volcanol. Geotherm. Res.*, *122*, 149–164, doi:10.1016/S0377-0273(02)00499-7.
- Nakano, M., H. Kumagai, B. Chouet, and P. Dawson (2007), Waveform inversion of volcano-seismic signals for an extended source, *J. Geophys. Res.*, *112*, B02306, doi:10.1029/2006JB004490.
- Nakano, M., H. Kumagai, and H. Inoue (2008), Waveform inversion in the frequency domain for the simultaneous determination of earthquake source mechanism and moment function, *Geophys. J. Int.*, *178*, 1000–1011, doi:10.1111/j.1365-246X.2008.03783.x.
- Neuberg, J., R. Luckett, M. Ripepe, and T. Braun (1994), Highlights from a seismic broadband array on Stromboli volcano, *Geophys. Res. Lett.*, *21*(9), 749–752, doi:10.1029/94GL00377.
- Nishimura, T. (2004), Pressure recovery in magma due to bubble growth, *Geophys. Res. Lett.*, *31*, L12613, doi:10.1029/2004GL019810.
- Nishimura, T., H. Nakamichi, S. Tanaka, M. Sato, T. Kobayashi, S. Ueki, H. Hamaguchi, M. Ohtake, and H. Sato (2000), Source process of very long period seismic events associated with the 1998 activity of Iwate Volcano, northeastern Japan, *J. Geophys. Res.*, *105*(B8), 19,135–19,417, doi:10.1029/2000JB900155.
- Ohminato, T. (2006), Characteristics and source modeling of broadband seismic signals associated with the hydrothermal system at Satsuma-Iwojima volcano, Japan, *J. Volcanol. Geotherm. Res.*, *158*, 467–490, doi:10.1016/j.jvolgeores.2006.08.004.
- Ohminato, T., and B. A. Chouet (1997), A free-surface boundary condition for including 3D topography in the finite-difference method, *Bull. Seismol. Soc. Am.*, *87*, 494–515.
- Ohminato, T., B. A. Chouet, P. Dawson, and S. Kedar (1998), Waveform inversion of very long period impulsive signals associated with magmatic injection beneath Kilauea Volcano, Hawaii, *J. Geophys. Res.*, *103*(B10), 23,839–23,862, doi:10.1029/98JB01122.
- Phillips, S., and K. Aki (1986), Site amplification of coda waves from local earthquakes in central California, *Bull. Seismol. Soc. Am.*, *76*, 627–648.
- Sakamoto, Y., M. Ishiguro, and G. Kitagawa (1986), *Akaike Information Criterion Statistics*, 320 pp., D. Reidel, Dordrecht.
- Sparks, R. S. J. (1978), The dynamics of bubble formation and growth in magmas: A review and analysis, *J. Volcanol. Geotherm. Res.*, *3*, 1–37, doi:10.1016/0377-0273(78)90002-1.
- Takemura, S., T. Furumura, and T. Saito (2009), Distortion of the apparent S-wave radiation pattern in the high-frequency wavefield: Tottri-Ken Seibu, Japan earthquake of 2000, *Geophys. J. Int.*, *178*, 950–961, doi:10.1111/j.1365-246X.2009.04210.x.
- Waite, G. P., B. A. Chouet, and P. B. Dawson (2008), Eruption dynamics at Mount St. Helens imaged from broadband seismic waveforms: Interaction of the shallow magmatic and hydrothermal systems, *J. Geophys. Res.*, *113*, B02305, doi:10.1029/2007JB005259.
- Wegler, U. (2003), Analysis of multiple scattering at Vesuvius volcano, Italy, using data of the TomoVes active seismic experiment, *J. Volcanol. Geotherm. Res.*, *128*, 45–63, doi:10.1016/S0377-0273(03)00246-4.
- Wegler, U., and B.-G. Lühr (2001), Scattering behaviour at Merapi volcano (Java) revealed from an active seismic experiment, *Geophys. J. Int.*, *145*, 579–592, doi:10.1046/j.1365-246x.2001.01390.x.
- Wessel, P., and W. H. F. Smith (1998), New improved version of generic mapping tools released, *Eos Trans. AGU*, *79*, 579, doi:10.1029/98EO00426.
- Yamasato, H. (1997), Quantitative analysis of pyroclastic flows using infrasonic and seismic data at Unzen Volcano, Japan, *J. Phys. Earth*, *45*, 397–416.
- S. Arrais, P. Palacios, M. Ruiz, M. Vaca, and H. Yepes, Instituto Geofísico, Escuela Politécnica Nacional, Ladrón de Guevara E11-253, Apartado 2759 Quito, Ecuador.
- H. Kumagai, M. Nakano, and T. Yamashima, Earthquake Research Department, National Research Institute for Earth Science and Disaster Prevention, 3-1 Tennodai, Tsukuba, Ibaraki 305-0006, Japan. (kumagai@bosai.go.jp)
- T. Maeda, Center for Integrated Disaster Information Research, Interfaculty Initiative in Information Studies, The University of Tokyo, 7-3-1 Hongo, Bunkyo-ku, Tokyo 113-0033, Japan.
- I. Molina, Institut des Sciences de la Terre d'Orléans, Campus Géosciences 1A Rue de la ferronnerie, 45100 Orléans Cedex 2, France.